Meteorol. Z. (Contrib. Atm. Sci.), Early Access DOI 10.1127/metz/2023/1153

Early Access Article

Characteristics and phenomena of the urban climate

Dedicated to Tim R. Oke for his outstanding achievements to urban climatology

Wilhelm Kuttler[1*] and Stephan Weber[2]

[1]University of Duisburg-Essen, Campus Essen, Faculty of Biology, Applied Climatology, Essen, Germany
[2]Climatology and Environmental Meteorology, Institute of Geoecology, Technische Universität Braunschweig, Germany

(Manuscript received June 8, 2022; in revised form November 30, 2022; accepted December 1, 2022)

Abstract

The urban climate is a modified boundary layer climate that is directly and indirectly influenced by anthropogenic activity and characterized by phenomena such as urban warming, reduced evapotranspiration, and increased emission of pollutants. As more than half of the global population is urban and the impacts of climate change will increase pressure on cities, a thorough understanding of the urban climate-related processes and phenomena is of vital importance. The present contribution gives a contemporary overview of the characteristics and phenomena of the urban climate addressed to non-specialists in the field. Starting with an analysis of the general differences between large cities and their surrounding environments, important aspects such as the radiation, energy and water balance as well as the temperature distribution in cities are presented in detail. Additionally, the situation of urban air quality and human–biometeorological aspects are described and the impact of climate change are addressed. Finally effective local adaptation and mitigation measures to reduce urban warming and flooding due to heavy rainfall are discussed.

Keywords: Urban climate, urban meteorology, urban ecosystem, global climate change

1 Introduction

Urban climatology is a subject of the research field 'Applied Climatology and Environmental Meteorology' and deals with the energetic, dynamic and material interactions between the near-surface atmosphere and the urban environment on the micro- and mesoscale. Cities show characteristic thermal, hydrological and airflow modifications in comparison to their surroundings depending on their morphology, the allocation and mixture of natural and built-up areas, the degree of sealing, the emission of heat, water, air pollutants and greenhouse gases as well as the prevailing weather type. The geographical location and the socio-economic conditions of a country also directly or indirectly influence the cities' climate.

Urban climatology deals with the spatio-temporal analysis and prediction of the local climate and air quality as well as the influence on urban inhabitants, e.g., by analysing the human–biometeorological impact. Urban climate effects appear worldwide to very different degrees and are influenced by and embedded in the regional background climate. This justifies a distinction between different types of urban climates, such as those in coastal, mountainous or lowland locations. To take this variation into account, the plural "urban climates" is sometimes used instead of speaking of "urban climate" in general terms (e.g., Oke et al., 2017).

*Corresponding author: Wilhelm Kuttler, University of Duisburg-Essen, Campus Essen, Faculty of Biology, Applied Climatology, 45127 Essen, Germany, e-mail: wikutt@outlook.de

This paper presents a contemporary overview of the characteristics and phenomena of the urban climate addressed to non-specialists in the field. Given the grand challenges of worldwide urbanisation and the increasing pressure on cities due to climate change, many applied working fields such as urban planning and urban mobility will benefit from a better knowledge of urban climate effects. This may help to better take into account certain trade-offs between aspects in their own working fields and urban climate related effects. An in-depth overview of the methodological aspects of urban climate data acquisition such as field (stationary and mobile) observations (e.g. Foken, 2021), physical (wind tunnel) modelling (e.g. Cermak et al., 1995) and numerical modelling (e.g. Gross and Etling, 2003, Masson et al., 2020a, b; Sharma et al., 2021) will not be explicitly given. Nevertheless, their results are vital for the qualitative and quantitative description of urban climate conditions. The majority of observation results of urban climate effects may not be from large networks spanning entire urban areas (e.g., Rotach et al., 2005; Scherer et al., 2019) but from single or multiple sites that are installed for project-specific research purposes. Although results from these single-point observations are not generally transferable to other cities/sites they very often depict processes and patterns that are valid in other cities under similar conditions, e.g., site characteristics.

Urban meteorology is to be distinguished from urban climatology. The former is used when, for example, studies look into short-term physical, chemical, and biological processes or forecast urban weather or air qual-

Table 1: Structural and climatic differences between sealed urban and flat, natural surrounding areas (generalized data for an example central European city).

Parameter	Typical modifications compared to the surrounding area
Surface	"3D" city versus "2D" hinterland; thus increase of urban surface; in addition, strong horizontal and vertical sealing
Material/subsoil	High material density, thermal conductivity and heat capacity ("storage capacity"); due to sealing: altered water balance (runoff increase, evaporation restriction), lower cooling due to reduced latent heat flux, loss of natural cold-air formation areas
Radiation	Impairment of all radiation balance elements depending on the respective reflectance and emissivity; influence of the geometry of the street canyons (house heights/street width ratio) on radiation transport (including UV-radiation); increased long-wave radiation $L\uparrow$ due to higher surface temperatures, lower effective radiation in narrow streets
Energy balance	Sensible turbulent heat flux Q_H higher than latent heat flux Q_E, thus higher air temperature; additional emission of "anthropogenic heat" Q_F by industry, commerce, building air conditioning, motor vehicles, human metabolism
Temperature	Higher surface temperature during the day and at night as well as higher air temperature with formation of corresponding heat islands (UHI) especially at night
Air humidity	Lower due to reduced rainwater infiltration and limited evapotranspiration; higher in individual cases, however, depending on weather conditions (UME = urban moisture excess); lower number of foggy days
Precipitation	Case-by-case increase in rainfall downwind of cities; reduction in the number of snow days and the frequency and quantity of dewfall
Wind	Decrease in wind speed, thus reduced air exchange; increase in gustiness and turbulence intensity (direction and speed) at or near building edges; jet effects in street canyons
Air pollutants	Predominantly higher concentrations (solid, liquid, gaseous) due to emissions from motor vehicles, commerce, industry, domestic heating; filtering and absorption function of gaseous and particulate air pollutants by vegetation; emission of biogenic hydrocarbons (BVOC) from certain plants as ozone precursor gases; strong release of greenhouse gases (H_2O_{gas}, CO_2, CH_4, etc.)
Impact on humans	Increased due to higher summer heat, day and night (e.g. heatwaves); generally higher noise pollution and poorer air quality

ity. Both can differ significantly from the surrounding area due to building development and the emission of heat and air pollutants. As an early warning system, one will want to rely on small-scale potential disaster forecasts, such as flooding as a result of a local heavy precipitation event, heavy fog, heat waves or air pollution that exceeds threshold values (e.g., Baklanov et al., 2018; Grimmond et al., 2015). In practice, conceptual distinctions between urban climatology and urban meteorology are often not drawn, but often used synonymously. The focus of this paper will be less on addressing the problems of urban meteorology but on those of urban climatology, the latter discipline being dedicated to the statistics of the measured variables and their quantitative description.

2 Characteristics of the urban climate

In this paper, characteristic differences in climate and air quality between a city and its rural environment are explained, mainly using examples of large cities in the mid-latitudes. Unless otherwise specified, the surrounding area is taken to be the area around a city that, for comparative purposes, reflects the regional background climate of the region. Generally, urban areas may be distinguished from their surrounding by urban overheating, i.e. by higher surface and air temperatures (cf. Table 1).

The mean urban wind speed is significantly reduced by the urban fabric and its roughness objects, resulting in a reduction of air mass exchange within the city as well as with the surrounding countryside. As a result, the nocturnal cooling and a removal of airborne pollutants are usually limited. However, wind gusts characterized by considerable fluctuation of wind direction and speed can be caused by the urban fabric, especially at building edges (corners, roofs, etc.).

With some exceptions, absolute humidity in cities generally has lower values than in the rural area. This occurs mainly due to the fact that, in the case of heavy sealing, the precipitation water is not only drained quickly, but usually also protected against evaporation in canal systems running underground. The much higher number of foggy days per year observed decades ago, especially in industrial regions, has greatly decreased due to the improvement of air quality and also as a result of the increase in urban overheating (Vautard et al., 2009).

The urban climatic characteristics are particularly pronounced during so-called "autochthonous" weather conditions. This is characterized by strong daytime insolation, weak winds and stable atmospheric stratification

during the night. In winter such conditions are occasionally accompanied by surface fog or elevated fog.

2.1 Characteristics of the urban morphology

The three-dimensional urban fabric significantly influences aerodynamic, thermal, hydrological as well as air-pollution conditions. To characterize the morphological properties of the urban area, different parameters are considered. These include urban cover, length scales and urban structures. Details of the most commonly used metrics are given in Fig. 1 and Table 2.

In addition to the canyon aspect ratio, λs, the sky view factor (ψ_{sky}) is used. The latter index represents a measure of the proportion of the restriction to the maximum possible unobstructed sky view. Thus, with $\psi_{sky} = 0$ ($\hat{=}\,0\,\%$ unobstructed view) and with $\psi_{sky} = 1.0$ ($\hat{=}\,100\,\%$ unobstructed view), appropriate constraints are set. Finally, the increase and arrangement of buildings (2D → 3D) in combination with the different thermal behaviour of urban compared to natural materials (cf. Chapter 5) modifies the climatic conditions in urban areas.

To analyse the climate of a city, representative land-use and urban structure types were defined. For such a classification, the term "climatope" (VDI RL 3787 Part 9) was first used in Germany, later also in Japan. A climatope is defined as an "area with similar microclimatic characteristics", which is given by aerodynamic surface roughness, the topographical setting as well as the type of land-use (VDI RL 3787 Part 1, p. 4).

The climatope classification is based on land-use type boundaries and the analysis of some representative measurements, hence giving a qualifying rather than quantifying definition. On an international level the latter is done by using land-use types ("landscape series"), which are determined by corresponding structural-physical indicators and thus represent a more precise means of area delimitation.

Appropriately employed properties include, ψ_{sky}, λi, mean flow obstacle height (z), surface albedo (α_d), heat transfer coefficient of surface materials (α), and anthropogenic heat flux (Q_F). Stewart and Oke (2012) use a selection of these properties to objectify their classification as so-called "local climate zones" (LCZs). The LCZ classification distinguishes 10 types of built-up areas (from "compact highrise" to "open midrise" to "heavy industry") and seven undeveloped surface cover types (from "dense trees" to "low plants" to "water"). The LCZs have been used in a wide range of urban climate studies, including urban heat island analysis, and are characterized by extensive applicability in cities of different geographic contexts.

For example, the WUDAPT initiative (Worlds Urban Database and Access Portal Tools) uses the LCZ for the standardised description of urban morphology to support a unified urban geodata platform that can be used in urban climate model studies and analyses worldwide (Demuzere et al., 2021).

To capture and quantitatively describe the city, in addition to the micro-scale structural parameters mentioned in Figure 1 and Table 1, urban shape ("city size"), fractal dimension, which determines the compactness of a city, and anisometry are also used. The latter provides information about the extent of a city based on the calculation of the eccentricity (major to minor axis of an ellipse; Zhou et al., 2017). Generally, there is a growing need for high-resolution information on urban structure and morphology, e.g. for implementation in numerical models. A recent discussion on that topic is provided by Masson et al. (2020b).

2.2 Empirical estimation of urban climatic parameters

Urban climate and air pollution parameters measured in cities are basically to be understood as composite values (W), which consist of at least three individual components (H, T, U) (Lowry, 1977). These are a global climatic component determined by the large-scale geographic location and referred to as the background value (H), a regional component determined by topography and defined by surface form and land use (topography value T), and the influence attributable to the degree of urbanization (urbanization value U).

In Eq. (2.1) these terms are summarised:

$$W_{itx} = H_{itx} + T_{itx} + U_{itx} \tag{2.1}$$

with i = weather type, t = time of measurement, and x = location of the measurement site in the urban area.

In order to prove that the influence exclusively occurs due to urbanization, it would be necessary to compare current climate and air quality data with pre-urban observations for comparable weather conditions (so-called "before/after comparison"). However, such a procedure is hardly possible, since measurement data going back to the time before a city was founded and collected at the same location are usually not available. A well-known exception is probably the measurement series of the city of Columbia, Maryland, USA, for which continuous climate data recording already exists from the time before the city was founded. Since the data accompanied the city growth over years, a time- and thus size-dependent change of different urban climate parameters could be proven (Landsberg, 1979). Apart from such very rare exceptions, it is usually necessary to determine urban influences by other means. The following approaches are used:

- comparative measurements (pre-urban/urban) using urban models such as wind tunnel or numerical simulation,
- regression analysis for individual climate quantities as a function of the temporal development of the size of an urban area or, alternatively, of its number of inhabitants, or

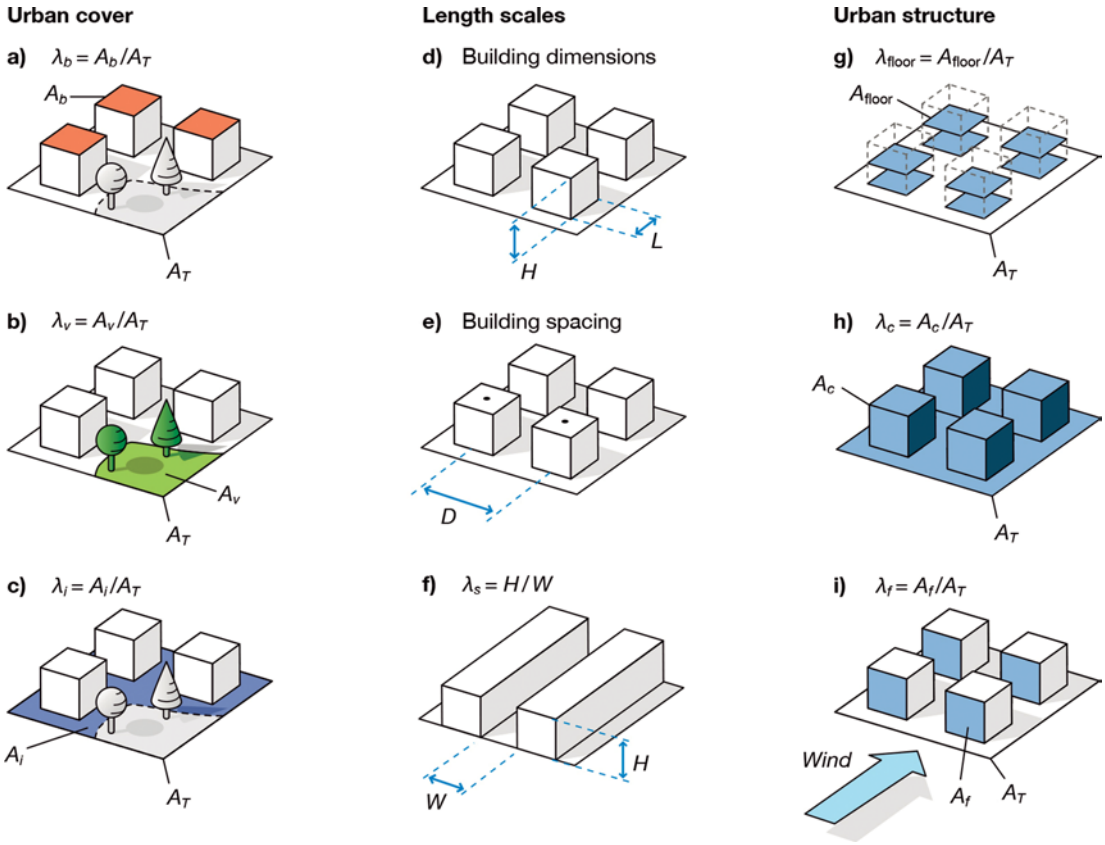

Figure 1: Parameters used to describe urban cover, length scales and urban structure (source: Oke et al., 2017).

Table 2: Explanation of the parameters of Fig. 1.

Urban cover	Length scales	Urban structure
a) $\lambda_b = \frac{A_b}{A_T}$ λ_b = plan area fractions of buildings A_b = plan area of buildings A_T = plan area of total surfaces	d) H = building height L = building length	g) $\lambda_{floor} = \frac{A_{floor}}{A_T}$ λ_{floor} = floor space ratio A_{floor} = floor space A_T = plan area of total surfaces
b) $\lambda_v = \frac{A_v}{A_T}$ λ_v = plan area fractions of vegetation A_v = plan area of vegetation A_T = plan area of total surfaces	e) D = distance between building centroids	h) $\lambda_c = \frac{A_c}{A_T}$ λ_c = complete aspect ratio A_c = complete surface area A_T = plan area of total surfaces
c) $\lambda_i = \frac{A_i}{A_T}$ λ_i = plan area fractions of impervious ground A_i = plan area of impervious ground A_T = plan area of total surfaces	f) $\lambda_s = \frac{H}{W}$ λ_s = canyon aspect ratio H = building height W = canyon width	i) $\lambda_f = \frac{A_f}{A_T}$ λ_f = frontal area aspect ratio A_f = frontal area A_T = plan area of total surfaces

- stationary/mobile measurements in urban and rural areas, where the comparison of the data is used to draw conclusions about the urban climate influence. Here, the correct placement of measuring stations both within the city and in the surrounding area is important, since the urban climate effect to be demonstrated depends to a considerable extent on the location of the measuring devices and the subsurface conditions (details on this, e.g., in Kuttler et al., 2015; VDI RL 3785, Part 1, 2; VDI RL 3787, Part 2, 9),
- measurements during "upwind-downwind situations" or to determine "weekday-weekend differences" (e.g., Oke et al., 2017). These approaches are mainly used in urban air quality studies.

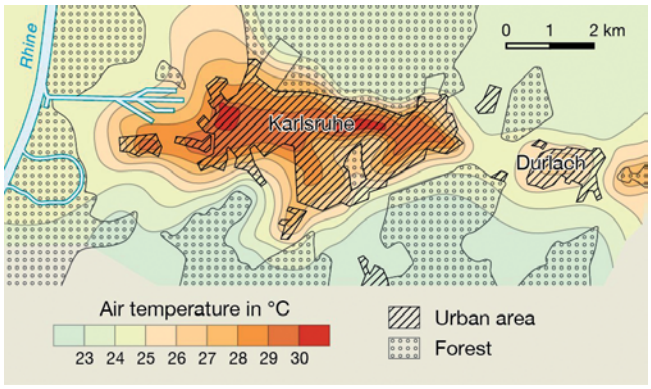

Figure 2: Results of an evening air temperature measurement in the Karlsruhe city area on 23 July 1929 (19:30–21:00, source: Peppler, 1930).

3 Historical aspects

The consideration of climate and air quality of the urban environment reaches back relatively far in history. Thus, about 2000 years ago, it was probably the Indians and Romans who first addressed the problem of overheating and air pollution in their burgeoning urban settlements (see, e.g., Neumann, 1979; Yoshino, 1990/91). The work of the Roman architect and civil engineer Marcus Vitruvius (75 B.C.–26 B.C.) compiled in "De Architectura libri decem" ("Ten Books on Architecture") summarizes the knowledge of the time about the design and structure of buildings and cities, with references to local climate and air quality. He gave the first indications of early urban planning, which was groundbreaking for the time (Fensterbusch, 1991). Significant attention to urban climatic and especially air-quality problems was given to the growing cities of the Middle Ages and modern times. London, for example, can be considered a prime example of a city with severe air pollution and resulting serious health problems among the population (Evelyn, 1661). Furthermore, a detailed study of the climate of London was carried out by Howard (1818).

In Paris, it was Emilien Renou (1815–1902) who took up the problem of reduced evening cooling of the urban fabric for which the term "Urban Heat Island" (UHI) was introduced later (obviously by Balchin and Pye, 1947).

Similar to the analysis of the urban climate, pioneering studies on the chemistry of the urban atmosphere were conducted as early as the end of the 19th century. In his 600-pages book "Air and Rain – The Beginnings of a Chemical Climatology", Robert Angus Smith (Smith, 1872) published detailed results of chemical analyses of urban air and precipitation quality (Smith is also known as the "Father of the Acid Rain").

A further development was the systematic research of partial aspects of the urban climate, which was initiated at the end of the 19th century mainly by German and Austrian scientists, such as Gustav Hellmann, August Schmauss and Julius Hann (e.g., Hann, 1885). The interest for an overall climatic synoptic analysis of cities increased at that time. First works on this subject were presented on Berlin (Behre, 1908) and Stuttgart (Knauss, 1901).

In addition to the purely scientific interest in urban climatology, applied-oriented urban planning experienced a strong upswing at the beginning of the 20th century, as impressively demonstrated by the publication of Karl Kassner with his paper "Die meteorologischen Grundlagen des Städtebaus" (Kassner, 1910), which was groundbreaking for the time.

An absolute innovation with regard to the inventory of methods used was represented by mobile measurements by means of motor vehicles first carried out by Wilhelm Schmidt in Vienna in 1927 (Schmidt, 1930) and by Albert Peppler in Karlsruhe in 1929 (Peppler, 1930). Both recorded the horizontal distribution of air temperature inside and outside a city (Fig. 2). This was the step from single point to spatially distributed measurements and also a first step towards horizontal urban air temperature distributions.

The multitude of international publications gradually prepared the ground for a first monograph on urban climate, presented as a dissertation by the German Benedictine priest Albert Kratzer in 1937. In the second edition of his book, he devoted himself to the problem of air quality in cities, in addition to changes in meteorological quantities (Kratzer, 1956).

Bioclimate research related to humans, nowadays called human-biometeorology, was systematically advanced in the middle of the 20th century. Among others, Weickmann et al. (1952) as well as F. Steinhauser, O. Eckel and F. Sauberer (e.g., Steinhauser et al., 1955, 1957, 1959) were involved. Decades later, an exemplary first "applied-oriented climatography" ("climate atlas") was prepared for the city of Vienna (Auer et al., 1989). The Metropolitan Meteorological Experiment (METROMEX) conducted in St. Louis, Missouri, USA, between 1971 and 1975 represents a major advance in the understanding of urban influences on precipitation patterns. As a result, both precipitation-increasing and thunderstorm-frequency-enhancing ur-

Table 3: Progress of urban climate research in the 20th/21st century (sources: Yoshino, 1990/91; Oke et al., 2017; supplemented and modified).

Early to mid-20th century
Predominantly descriptive climatographies of individual cities mid to late 20th century (e.g., Hupfer and Chmielewski, 1990 for Berlin)
Stormy development of urban climatology documented in numerous bibliographies, e.g., first annotated bibliographies on urban climatology (e.g., Brooks, 1952; Chandler, 1970; Oke, 1974, 1979)
Refinement and improvement of measuring instruments allowed better methodological differentiation of and stronger analytical approach to urban climate studies
Three-dimensional recording of climatic and air-hygienic parameters in the urban boundary layer
Increased use of remote sensing methods, numerical simulations and wind tunnel analysis
Preparation of urban climate maps, introduction of the term "climatope" (in Germany); emergence of urban climate atlases (Ren et al., 2011)
Analysis of urban precipitation
Qualitative and quantitative analysis of anthropogenic heat (industry, building heating, motor vehicle traffic, metabolic heat)
Classification of urban heat islands (subsurface, surface, atmospheric)
Increased implementation of urban climate analyses also in developing countries
Emergence of various bilingual guidelines of the Association of German Engineers (VDI RL) in the field of "environmental meteorology"
Process-oriented work on urban exchange processes (flux density measurements of meteorological quantities and air pollutants using the eddy covariance method)
Expansion of human-biometeorological research; creation of indicators for the thermal impact (e.g. PET, pt, UTCI); definition of limit values for the air-hygienic impact complex
Late 20th century / early 21st century
Urban climate and global climate change: mitigation and adaptation strategies for cities
Increased emergence of spatially high-resolution numerical models for urban meteorological forecasts (e.g., URBMET = Urban Meteorology, Bornstein, 1975; TEB = Town Energy Balance model, Masson et al., 2002; ENVIMET = Environmental Meteorology, Bruse, 1998; and the Parallelized LES Model PALM for urban application (PALM-4U; Raasch and Schröter, 2001; Scherer et al., 2019) based on the Large Eddy Simulation LES). For a brief recent overview on urban microscale and mesoscale models the reader is referred to Masson et al. (2020a) and Hamdi et al. (2020).

ban effects were identified (Changnon, 1981). In the tropics/subtropics (Malaysia), Sani Sham in the 1970s (Sham, 1979, 1990), Ernesto Jauregui in Mexico (Jauregui, 1973), and the research group led by Matsumoto Moriyama of Japan (Moriyama, 1988) were among those who have explicitly addressed urban climate. For example, Moriyama introduced the urban climate planning aspect ("Climate Atlases for Cities") in Japan, following the German methodology. Nearly three decades after Albert Kratzer's dissertation, Helmut Landsberg's "The Urban Climate" in the 1980s presented another monograph on the subject in line with the state of knowledge at the time (Landsberg, 1981). In many places, the urban planning factor played an increasingly important role in application-oriented urban climate research, as evidenced by corresponding publications such as "Air Quality and Climate – A Handbook for Urban and Regional Planning" (Schirmer et al., 1993) and "Urban Climate and Air Pollution Control" (Helbig et al., 1999).

Against the background of the increased occurrence of smog episodes in some industrial areas of Central Europe (and also North America), especially since the mid-20th century the aspect of the "London Smog" and later the photochemical smog ("Los Angeles Type"), received more attention in the "air pollution climatology" (Kuttler, 1979a, b).

In particular, the work of Timothy R. Oke and the research he initiated in the second half of the 20th century pioneered the knowledge of urban climatology. The wealth of individual publications formed the basis for an outstanding textbook on urban climates written with other colleagues in the field (Oke et al., 2017). Individual projects, such as the one on "Urban Climate Bavaria" (Mayer, 1988), the Basel Urban Boundary Layer Experiment (BUBBLE, Rotach et al., 2005), CAPITOUL in Toulouse (Masson et al., 2008), URBAN 2003 (Allwine et al., 2004), and 3-DO in Berlin (Scherer et al., 2019) led to a better understanding, especially of the three-dimensional complex processes occurring within the urban atmosphere (see also Table 3).

Since the 1970/80s, human-biometeorological research has significantly progressed. This is because previously existing, less meaningful indicators based purely on physical principles have been replaced by much more suitable standards of effectiveness that not only take

into account the physiological processes of the human body as a function of different stress conditions but can also vary different levels of clothing (e.g., Jendritzky et al., 1979; Mayer and Höppe, 1987). In light of the widespread use of increasingly sophisticated stationary [e.g., crowdsourcing (Chapman et al., 2016, Meier et al., 2017, Droste et al., 2020)] and mobile measurement technologies [e.g., drones, UAV (Naughton and McDonald, 2019; Smith et al., 2021)], the advancement of numerical-mathematical and physical modelling (wind tunnel), and the improvement of satellite measurements, applied urban climatology as a practice-oriented subdiscipline increasingly emerged. In Germany, for example, applied-oriented results have not only been reflected in a multitude of publications, but also find their way into German legal regulations as well as into various practice-oriented, bilingually published guidelines of the Association of German Engineers (VDI), in particular in the guidelines on environmental meteorology (e.g., VDI 3785, 3787, 3789, each with numerous parts).

Especially in times of global climate change, not only the fundamental research, but particularly the applied urban climate research is of vital importance. However, it is still under debate in how far results from scientific studies (mainly in English) address the needs of municipal/local authorities. Practice even shows that the hurdle to using and understanding non-native scientific texts may still be rather high for institutions in applied urban planning.

4 Structure of the urban atmosphere

The complexity of the urban fabric, given by the three-dimensional structure of the built-up area, leads to characteristic effects on the vertical structure of the lower atmosphere, defined as the urban boundary layer (UBL). Under the condition of cloudless, dry (autochthonous) weather, this layer can reach a height of 1 km to 2 km and is separated from the troposphere by a capping inversion. The vertical structure of the UBL can be subdivided as follows:

There are two main layers, the upper one (mixing layer), which is characterized by thermal turbulence (around 90 % of the total urban boundary layer) and the lower section (surface layer), which is more strongly influenced by mechanical turbulence (surface roughness) and only takes up about 10 % of the total thickness (Christen, 2019; Fig. 3).

In the surface layer, the flux densities of momentum, heat and humidity are considered quasi-constant with height. Here, mechanical turbulence predominates due to friction. Depending on the building structure, the surface layer can be subdivided into an urban canopy layer (UCL) extending from the Earth's surface to the average building height followed by the urban roughness sublayer (URS) and the inertial sublayer. While the flow conditions in the UCL are influenced by individual buildings and the structure of street canyons, for the

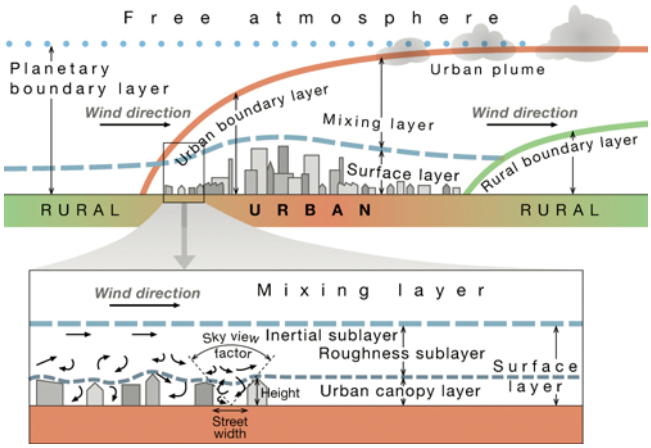

Figure 3: Modification of the planetary boundary layer by a city (strongly generalised; source: Oke, 1997, cited in Kuttler, 2013, modified).

URS the influence of entire groups of buildings or city quarters is decisive. In the inertial sublayer the flow is in equilibrium with the urban roughness so that turbulence is 'quasi-homogeneous'. Depending on the wind direction, the airflow in both layers is determined by advection and varying degrees of mechanical and thermal turbulence (gustiness), the causes of which can be seen in the position, size and distance of individual buildings from each other as well as their thermal properties, e.g. as expressed by ψ_{sky} (cf. Section 2.1).

The vertical structure of the urban atmosphere is modified by the prevailing wind direction and speed. By this, their height in the wind direction depends on the roughness differences between the surrounding area and the city, depending on the strength of the interactions with the underlying layer.

Ideally, UBL height reaches a maximum above the city and adjusts to the rural surface conditions beyond the urban boundaries. However, above the rural boundary layer, the urban plume can persist for several kilometers under appropriate wind conditions and, depending on turbulence, reach the ground before it finally dissipates. In some cases, this may impact rural air quality downwind of urban areas due to the transport of urban air pollutants.

The urban atmospheric stratification is characterized by (slightly) unstable conditions during the day, but by rather neutral or slightly stable conditions at night (Christen and Vogt, 2004; Weber and Kordowski, 2010).

These results show that the UBL, especially during the day, but also at night, often has a larger mixing volume than the rural boundary layer. Hence, air pollutants can be more strongly dispersed within an urban area. The maximum height of the mixing layer depends not only on the intensity of solar radiation, but also on soil moisture (because of its influence on heat transport) and, of course, on the time of year (Fig. 4, Marley et al., 2021).

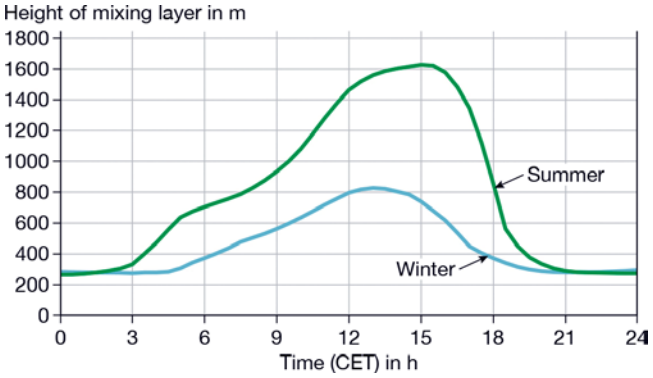

Figure 4: Diurnal variation of mixing layer heights in summer and winter over Vienna (calculated from ceilometer data 07/2013–06/2014; source: Lotteraner and Piringer, 2016; modified).

The atmospheric exchange in the city is reduced compared to the surrounding area due to the usually significantly lower wind speed within the urban roughness layer, which can favour the accumulation of airborne pollutants and heat. However, individual roughness elements can promote directional and velocity gustiness as well as increased turbulence intensity due to the formation of edge and wake vortices. Although locally this leads to a more effective mixing of the air, it can also cause high wind speeds, which are associated with reduced wind comfort (e.g., VDL RL 3787, Part 4).

Because cities are warmer than their surrounding areas (see Section 5.1), thermal circulations can develop between the city and the surrounding area during clear and calm weather conditions. Because of its thermal origin, the flow is known as Urban Heat Island Circulation (UHIC). This microscale, ground-level, converging flow occurs intermittently with low wind speeds (< 2 m/s) and penetrates from the surrounding area into an urban body – but only under optimal conditions. In urban areas, the wind speed can be occasionally higher (Dütemeyer, 2000). However, the penetration depth of this weak flow is not only dependent on meteorological conditions, but also in particular on the design of corresponding low roughness airflow paths, which, among other characteristics, should have only very low roughness lengths (z_o) and displacement-layer heights (d_o) (Mayer et al., 1994, Grunwald et al., 2019). In the upper part of the UBL, a correspondingly divergent flow from the city to the surrounding area exists. The horizontal extent of this wind system can be much larger than the city diameter (Hidalgo et al., 2008). Often clouds are generated by this wind system over the city (Theeuwes et al., 2022). The concept is outlined in Fig. 5.

5 Urban radiation and energy balance

The urban energy balance is influenced by the geographical location of a city on the macro-scale, by their size, structure and emission of pollutants on the meso-scale as well as by material and surface properties on the micro-scale. Furthermore, the prevailing weather conditions have a major influence. For example, urban climate phenomena can be particularly pronounced during clear and calm weather.

5.1 Radiation balance

The simplified radiation balance (Q^*) for the ground surface (with no storage capacity) and not affected by advection is as follows (Eq. (5.1)):

$$Q^* = (K\downarrow + L\downarrow) - (K\uparrow + L\uparrow) \quad \text{(all in W m}^{-2}\text{)} \quad (5.1)$$

with $K\downarrow$ = shortwave downward radiation flux density (direct and diffuse components) and $L\downarrow$ = long-wave downward radiation, and the output terms: $K\uparrow$ = shortwave upward and $L\uparrow$ = long-wave upward. According to the sign convention, flux densities towards the surface are defined as positive and those directed into the atmosphere as negative.

The shortwave downward flux density ($K\downarrow$ for wavelengths $\lambda \leq 3,000$ nm), which can be reduced in cities depending on the degree of atmospheric pollution, also subsumes UV radiation (295 nm $\leq \lambda \leq$ 385 nm), which is responsible for the production of vitamin D in humans. However, exposure to high UV doses may result in health problems (i.e., sunburn, skin cancer). The strength of UV radiation is not only dependent on the zenith angle of the sun and the degree of atmospheric pollution but is also influenced by the orientation of urban street canyons and ψ_{sky} (Wright et al., 2020). Hence, urban UV radiation can be reduced by up to 60 %, also due to the limited surface reflection of UV (Seckmeyer and Schrempf, 2018).

The albedo (α_d) differs on average only slightly between a city and its surrounding area. A lower urban $\alpha_{d,urb}$ value, however, can occur in winter, when snow and ice thaw more quickly in the warmer urban fabric.

The long-wave radiation flux densities ($L\downarrow$, $L\uparrow$) are determined by the temperature of the atmosphere (depending on the concentration of greenhouse gases) and the surface and the corresponding emissivities (ε).

The longwave upward radiation flux density $L\uparrow$ is determined by the surface temperature T_s, the surface ε as well as by ψ_{sky}. Due to variation of the three-dimensional urban surface and the reflection of atmospheric long-wave radiation from building walls, the influence on the long-wave radiation must be extended to $L\uparrow = \varepsilon\sigma T^4 + (1 - \varepsilon)L\downarrow$. For example, narrow street canyons (e.g. $\psi_{sky} = 0.3$) result in a significant increase in night-time $L\downarrow$ (Fig. 6; here about 75 W m^{-2}) and thus in a reduction of effective radiation (L^*), whereas in the case of wide canyons (e.g. $\psi_{sky} = 0.9$) this value may drop to only 10 W m^{-2}.

Artificial building materials in cities can have very different ε-values, which have a decisive influence on $L\uparrow$ and thus L^*. For example, most metal have very low

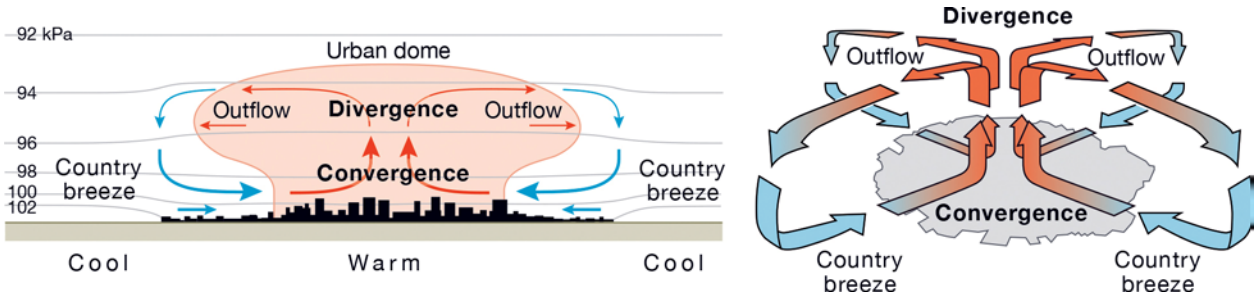

Figure 5: Schematic of the urban heat island circulation (UHIC). Left: Idealized 2D air pressure distribution. Thick lines are the resulting circulation. Right: Highly simplified view of the 3D circulation pattern, neglecting the Coriolis force (source: Oke et al., 2017).

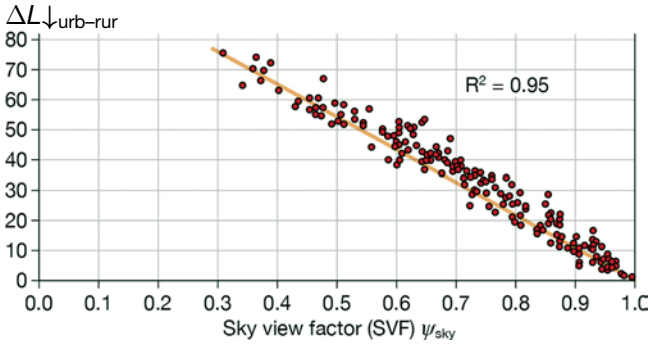

Figure 6: Dependence of the nocturnal increase in long-wave downward radiation compared to the surrounding area value ($\Delta L{\downarrow}_{\mathrm{urb-rur}}$) on the sky view factor (ψ_{sky}) during cloudless weather (data basis: eight nocturnal measurement runs, Krefeld, summer 2003; source: Blankenstein and Kuttler (2004, modified).

Table 4: Mean radiation budget components for urban and rural sites in Essen (06/2012–05/2013; radiation totals for the day in MJ m^{-2} d^{-1}, source: Kuttler et al., 2015).

Radiation component	Urban	Rural
$K{\downarrow}$	9.3	9.8
$K{\uparrow}$	1.1	1.6
$L{\downarrow}$	28.3	28.9
$L{\uparrow}$	32.7	31.7
Q^*	3.8	5.4

emissivity values <0.1 compared to building materials that almost reach black body values with $\varepsilon = 0.98$ (see, among others, Zmarsly et al., 2007). This means, for example, that the heating or cooling of materials can occur very differently.

Annual mean values of the radiation balance

The annual mean values of the urban radiation balance of a (sealed) inner city and a non-sealed surrounding area show the following differences (Table 4):

The mean $\alpha_{d,\mathrm{urb}}$ is about 5 % lower than in the surrounding area. This difference is probably caused by multiple or total reflections occurring in street canyons.

Furthermore, $K{\downarrow}$ might be slightly reduced (5 %) due to air pollution. $L{\downarrow}$ is slightly increased in the surrounding area, which can possibly be attributed to the higher water vapour content of the rural boundary layer. In the city, however, $L{\uparrow}$ ($L{\uparrow}_{\mathrm{urb}} = 32.7\,\mathrm{MJ\,m^{-2}\,d^{-1}}$ resp. $= 378\,\mathrm{W\,m^{-2}}$) is higher than in the rural area ($L{\uparrow}_{\mathrm{rur}} = 31.7\,\mathrm{MJ\,m^{-2}\,d^{-1}}$ resp. $= 367\,\mathrm{W\,m^{-2}}$), as urban areas are usually warmer than their surroundings.

While the short-wave radiation balances (K^*) hardly differ between the city and the surrounding area, larger differences can be seen for the long-wave radiation balance (L^*), which in the city reaches about 1.5 times the rural value. With regard to the total radiation balance, that of the urban site ($Q^*_{\mathrm{urb}} = 3.8\,\mathrm{MJ\,m^{-2}\,d^{-1}} \mathrel{\hat{=}} 45\,\mathrm{W\,m^{-2}}$) is significantly lower compared to that of the surrounding site ($Q^*_{\mathrm{rur}} = 5.4\,\mathrm{MJ\,m^{-2}\,d^{-1}} \mathrel{\hat{=}} 61\,\mathrm{W\,m^{-2}}$). Thus, on an annual average, less energy is released at the city site with $Q^*_{\mathrm{urb}} = 1,387\,\mathrm{MJ\,m^{-2}\,a^{-1}} \mathrel{\hat{=}} 385\,\mathrm{kWh\,m^{-2}\,a^{-1}}$ than is the case in the surrounding area ($Q^*_{\mathrm{rur}} = 1,971\,\mathrm{MJ\,m^{-2}\,a^{-1}} \mathrel{\hat{=}} 548\,\mathrm{kWh\ m^{-2\,-1}}$). However, this must not be a general feature at urban sites. Christen and Vogt (2004) report that although all terms of the radiation balance show some urban modification at their site, the resulting radiation balance Q^* at the top of the UCL shows little urban-rural difference.

5.2 Energy balance

The energy balance for the surface/atmosphere interface in the urban built-up area, which is considered to be without storage capacity, is shown here for weather without rain and wind, as follows (Eq. (5.2)):

$$Q^* + Q_F = Q_H + Q_E + \Delta Q_S \quad (\mathrm{in\ W\,m^{-2}}) \qquad (5.2)$$

with Q^* = radiation balance, Q_H, Q_E = turbulent sensible and latent heat flux densities, ΔQ_S = storage heat flux density of underground, buildings, and air volume between buildings, Q_F = anthropogenic heat flux density (emissions from motor vehicles, commerce, building air conditioning, industry, human metabolism).

The signs of the fluxes are positive when directed into the atmosphere, whereas they are negative when directed towards the surface.

Sensible and latent heat flux densities (Q_H and Q_E)

The turbulent sensible and latent heat fluxes can be related as Bowen ratio ($\beta = Q_H/Q_E$). Dry and sealed

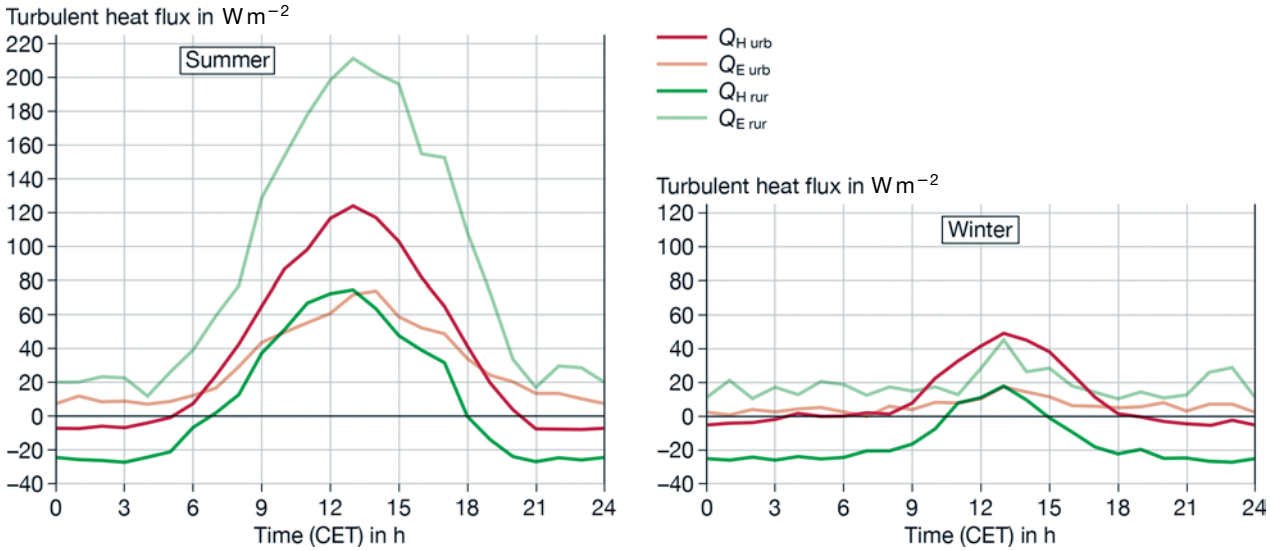

Figure 7: Daily average summer and winter turbulent heat flux densities in Oberhausen, Germany (06/2012–05/2013; source: KUTTLER, 2013; modified).

Table 5: Mean energy budget components for urban and rural sites in Essen (06/2012–05/2013; energy totals for the day in MJ m^{-2} d^{-1}, source: KUTTLER et al., 2015)

	Urban	Rural
Q_H	2.5	1.0
Q_E	1.4	4.4
β	1.8	0.2

surfaces that release energy predominantly via Q_H are characterized by β-values > 1. For moist soil surfaces or vegetation stands that are sufficiently supplied with water β is usually < 1. The specification of β thus allows a simple classification of different land use with regard to the prevailing heat exchange.

In order to reduce or avoid urban overheating, surfaces should have β-values < 1. This would ensure that turbulent energy is mainly exchanged via evapotranspiration (ET) and is therefore not available for heating the air.

Annual mean of the urban energy balance

An overview of the annual mean values of the energy balance Q_H and Q_E terms for an inner city and surrounding location are given in Table 5. As the storage term (ΔQ_S), which will be discussed later, balances out over a longer period of time, it is set to zero here. The mean urban Bowen ratio is $\beta_{urb} = 1.8$ due to the dominant influence of $Q_{H\,urb}$. In the rural area, however, β_{rur} reaches a value of 0.2 due to the predominant latent heat flux density ($Q_{E\,rur}$). On average, about 200 mm a^{-1} of water could be evaporated in the city, in comparison to > 625 mm a^{-1} in the rural area.

Mean diurnal cycles in summer and winter

The diurnal evolution of turbulent heat fluxes (Q_H, Q_E) is shown for a mean summer and winter day in Fig. 7. In summer, the mean rural Q_E – with sufficient water supply to the soil – represents the highest value of the heat fluxes of both sites during midday with $Q_{E\,rur} > 200\,W\,m^{-2}$. Thus, it is about three times compared to the urban value. In contrast, the sensible heat flux ($Q_{H\,rur} < 80\,W\,m^{-2}$) reaches a lower maximum value. The lower rural values are due to the fact that sufficient water for evaporation is usually available, e.g. so-called "blue-green" areas. These are vegetated areas that ideally have sufficient water supply at all times (details in ANTOSZEWSKI et al., 2020). At the urban site, the midday maximum for $Q_{E\,urb}$ is only $< 80\,W\,m^{-2}$ and thus roughly corresponds to $Q_{H\,rur}$ of the surrounding area, whereas more than 120 W m^{-2} are emitted to the atmosphere via $Q_{H\,urb}$.

During night-time, the latent heat fluxes are still positive in the urban and rural areas, so that a small but steady amount of water is evaporated into the nocturnal atmosphere. In contrast, the nocturnal sensible heat fluxes in both the city ($Q_{H\,urb}$, to a lesser extent) and the surrounding area ($Q_{H\,rur}$, to a greater extent) are negative and thus directed towards the surface. The higher negative $Q_{H\,rur}$ of the surrounding area are caused by a stronger temperature gradient (inversion) between the atmosphere and the much cooler surface than at the urban site. However, for a number of urban sites nocturnal Q_H values were reported to stay slightly positive overnight due to release of heat from the urban fabric.

In winter, the absolute values at both locations are lower than in summer due to the greater zenith distance of the sun. Thus, during the day a maximum of about 40 W m^{-2} is observed for $Q_{H\,urb}$, whereas the corresponding $Q_{E\,urb}$ value is 20 W m^{-2}. At night, both values drop to zero or into the slightly negative range. In the surrounding area, $Q_{E\,rur}$ is the dominating factor – although the absolute values are low. $Q_{H\,rur}$ only reaches slightly positive values here during the midday hours,

Table 6: Thermal properties of artificial and natural materials (source: Zmarsly et al., 2007).

Material		Density $\rho = \mathrm{kg \cdot m^{-3}}$	Specific heat $c = \mathrm{J \cdot kg^{-1} \cdot K^{-1}}$	Heat capacity $\zeta = \mathrm{J \cdot m^{-3} \cdot K^{-1}}$	Thermal conductivity $\lambda = \mathrm{W \cdot m^{-1} \cdot K^{-1}}$	Thermal diffusivity $a = \mathrm{m^2 \cdot s^{-1}}$	Thermal admittance $b = \mathrm{J \cdot m^{-2} \cdot s^{-0.5} \cdot K^{-1}}$
Asphalt		$2.11 \cdot 10^3$	$0.92 \cdot 10^3$	$1.94 \cdot 10^6$	0.75	$0.38 \cdot 10^{-6}$	1,205
Concrete	Porous –	$0.32 \cdot 10^3$	$0.88 \cdot 10^3$	$0.28 \cdot 10^6$	0.08	$0.29 \cdot 10^{-6}$	150
	Heavy concrete	$2.40 \cdot 10^3$	$0.88 \cdot 10^3$	$2.11 \cdot 10^6$	1.51	$0.72 \cdot 10^{-6}$	1,785
Brick		$1.83 \cdot 10^3$	$0.75 \cdot 10^3$	$1.37 \cdot 10^6$	0.83	$0.61 \cdot 10^{-6}$	1,065
Steel		$7.85 \cdot 10^3$	$0.50 \cdot 10^3$	$3.93 \cdot 10^6$	53.30	$13.60 \cdot 10^{-6}$	14,475
Glass		$2.48 \cdot 10^3$	$0.67 \cdot 10^3$	$1.66 \cdot 10^6$	0.74	$0.44 \cdot 10^{-6}$	1,110
Clay soil (40 % Pore-volume)	dry	$1.60 \cdot 10^3$	$0.89 \cdot 10^3$	$1.42 \cdot 10^6$	0.25	$0.18 \cdot 10^{-6}$	600
	saturated	$2.00 \cdot 10^3$	$1.55 \cdot 10^3$	$3.10 \cdot 10^6$	1.58	$0.51 \cdot 10^{-6}$	2,210
Water	4 °C still	$1.00 \cdot 10^3$	$4.18 \cdot 10^3$	$4.18 \cdot 10^6$	0.57	$00.14 \cdot 10^{-6}$	1,545

while the other daytime hours are characterized by negative $Q_{H\,\mathrm{rur}}$. As a result, sensitive heat from the warmer atmosphere is supplied to the colder surface.

In summary, the urban site is characterised by higher mean Bowen ratios in summer ($\beta_{\mathrm{urb}} = 1.5$) and winter ($\beta_{\mathrm{urb}} = 3.3$), while the values in the surrounding area range between $\beta_{\mathrm{rur}} = 0.3$ in summer and $\beta_{\mathrm{rur}} = 0.8$ in winter, thus documenting the clear advantage for rural evaporation. In the rural area the amount of Q_E may exceed that of Q^*, which leads to the well-known "oasis effect" ($Q^* < Q_E$, Vivoni et al., 2020).

Storage heat flux density (ΔQ_S)

ΔQ_S subsumes the absorption and release of energy from underground, buildings, and the air volume between buildings. Essentially, the strength of the flux density ΔQ_S is determined by the nature of the medium, in cities in particular by the building materials and their thermal properties, which can vary greatly (cf. Table 6).

Comparing the thermal admittance coefficients (b) of the most commonly used urban building materials being asphalt, concrete, brick, steel and glass, it is evident that most of the values, especially for steel, are considerably higher than b = 1,000 $\mathrm{J\,m^{-2}\,s^{-0.5}\,K^{-1}}$. Natural, dry clay soil has a comparatively low value of about 600 $\mathrm{J\,m^{-2}\,s^{-0.5}\,K^{-1}}$. High coefficients reduce T_s and conduct more of the absorbed energy into the material, thus delaying the occurrence of the maximum temperature by stronger damping. If the material is also characterised by high thermal conductivity and heat capacity (e.g. steel) a considerable amount of energy can be "absorbed".

Hourly distribution of the heat flux density terms

The question of how the net energy (Q^*) affects the turbulent fluxes during the course of the day will be examined focussing on Q_H, Q_E and Q_S as examples (Fig. 8). Urban and suburban values show very different but characteristic diurnal patterns.

Urban site: Between 30 % (21 h) and 70 % (8 h) of the daytime radiation balance is dissipated via Q_H. The range of $Q_{S\,\mathrm{urb}}/Q^*_{\mathrm{urb}}$ is 0.45 (21 h) and 0.0 (8 h). While about 45 % of net energy are stored in the urban fabric, it has been reduced to zero at sunrise indicating that stored energy has been released into the UBL overnight.

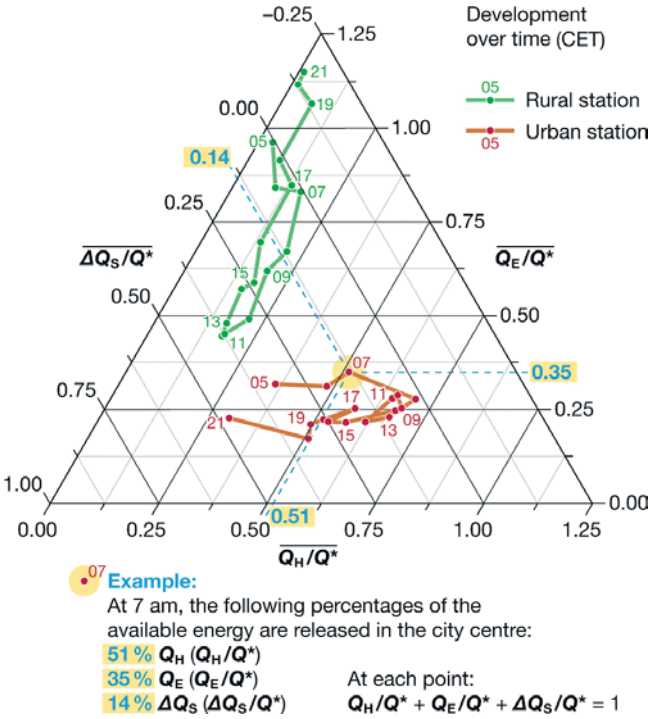

Figure 8: Diurnal variation of the mean hourly energy partitioning for an inner city and surrounding area site (near water bodies) in Essen (06/2012–05/2013) (source: Kuttler et al., 2015; modified) [$Q^* > 0\,\mathrm{W\,m^{-2}}$; ΔQ_S was determined residually from the energy balance].

The smallest difference with low absolute values during the course of day is the latent heat flux ($0.2 < Q_{E\,\mathrm{urb}}/Q^*_{\mathrm{urb}} \leq 0.35$), which is partly due to limited water availability. Only during the early morning hours slightly higher $Q_{E\,\mathrm{urb}}/Q^*_{\mathrm{urb}}$ ratios are observed, which may be due to evaporation of nocturnal dew.

Rural site: A rather vertically aligned diurnal sequence of energy distribution dominates. In contrast

Table 7: Mean share (in %) of different anthropogenic heat emission ($Q_{F\,elec}$, $Q_{F\,fuel}$, $Q_{F\,veh}$, $Q_{F\,met}$) and summer/winter means ($Q_{\Sigma F}$) in W m^{-2} (basis: 61 US-cities; source: Sailor et al., 2015).

	Electricity ($Q_{F\,elec}$ in %)	**Heating fuel** ($Q_{F\,fuel}$ in %)	**Vehicle** ($Q_{F\,veh}$ in %)	**Metabolism** ($Q_{F\,met}$ in %)	**Mean $Q_{\Sigma F}$** (in W m^{-2})
Summer	41	10	46	3	~08
Winter	25	40	33	2	~12

to the urban location, $Q_{E\,rur}$ reaches a relatively large range ($0.45 < Q_{E\,rur}/Q^*_{rur} \leq 1.15$). The evening value at 21 h exceeding 1 is compensated by $Q_{S\,rur}$, i.e. the ground heat flux density. The direct heating of the atmosphere by $Q_{H\,rur}$ accounts for a maximum of only 20 % ($0.0 < Q_{H\,rur}/Q^*_{rur} \leq 0.2$) over the entire course of the day, so that the rural near-surface boundary layer (in this case, however, near water bodies) remains cooler overall than the urban atmosphere.

Anthropogenic heat flux density (Q_F)

Q_F subsumes the waste heat generated by chemical or electrical technical processes of motor vehicles, power plants, industry, commerce or building air conditioning. This waste heat is emitted as radiant and turbulent heat. Metabolic heat ($Q_{F\,met}$), which is based on human or animal metabolism, is usually not included in the overall estimation of anthropogenic heat flux density due to its insignificance in relation to other compounds. However, this will be briefly discussed below.

Q_F is primarily determined by energy consumption, the urban structure and building type and the population density as well as the geographical location and topographical conditions of cities. Furthermore, of course, the prevailing climate type also influences energy consumption (Wienert and Kuttler, 2005). It is problematic that the literature has so far hardly used uniform data collection methods to calculate the corresponding data collectives, so that the comparability of the respective data is limited. At this point, global (horizontal resolution approx. 20 km^2, Allen et al., 2011) or local (horizontal resolution approx. 1 km^2, Lindberg et al., 2013) numerical Q_F-models can be used to improve the methodological comparability of the contributions of anthropogenic heat flux. The models usually explicitly resolve the individual contributions from the building sector, transport and metabolism. Table 7 contains examples of mean Q_F values on a comparable basis for a larger collective of US cities. According to this, the (comparatively low) average anthropogenic heat flux density, averaged over the entire urban area, amounts to about 8 W m^{-2} in summer and about 12 W m^{-2} in winter. This evaluation includes roughly equal proportions of cities characterized by both a winter and a summer climate, so that it represents a balanced picture of the Q_F situation for the cities of a western industrial nation.

The breakdown of anthropogenic heat fluxes shows that the largest share of energy is caused by the operation of motor vehicles and electricity-generating power plants in summer. In winter, heat emissions from the use of fossil fuels for heating buildings and the operation of motor vehicles dominate.

In both summer and winter, the share of Q_F attributable to human metabolism is low at ≤ 3 %. It must be taken into account that since people spend most of their time indoors, most of the energy is released here, which can have a lasting effect on the indoor energy balance.

The effect of Q_F on urban overheating, however, should not be underestimated. According to studies in American, Japanese and Russian cities, Q_F may increase not only air temperature but modifies also the pressure gradient and therefore wind speed (Flanner, 2009; Ginzburg and Dokukin, 2019). Furthermore, model-based analyses for Beijing, China, predict that by the year 2100 the anthropogenic urban heat emission is expected to increase, as are the number and duration of heat waves per year (Liu et al., 2021). This development could lead to an increased use of electrical energy for building cooling, which in turn could influence Q_F.

5.3 Temperature conditions in cities

As already explained, both surface and air temperatures in cities deviate from those of the surrounding area. The reasons for the occurrence and intensity of overheating are discussed below.

Urban heat island

The difference in air and surface temperatures between urban and rural areas is generally referred to as an "urban heat island" (UHI; $\Delta T = t_{urb} - t_{rur}$). In a highly generalized way, this designates the fact of an island-like urban overheating, usually with a positive sign, which is surrounded by a (usually) cooler area. In this context, it is also common to indicate a one-dimensional (horizontal) temperature gradient between the city and the surrounding area ($\Delta T\,m^{-1}$) = $t_{urb-rur}/\Delta x_{urb-rur}$ with x = distance in metres or kilometres. The gradient approach helps to identify heat cliffs (= spontaneously occurring temperature differences) between the city and the rural area. A more accurate description of the spatial occurrence of urban overheating, which is neither homogeneous in its intensity nor its spatial distribution, can usually be distinguished into several heat spots depending on building density. This may be referred to as the "heat archipelago", although this term has not become established in scientific literature.

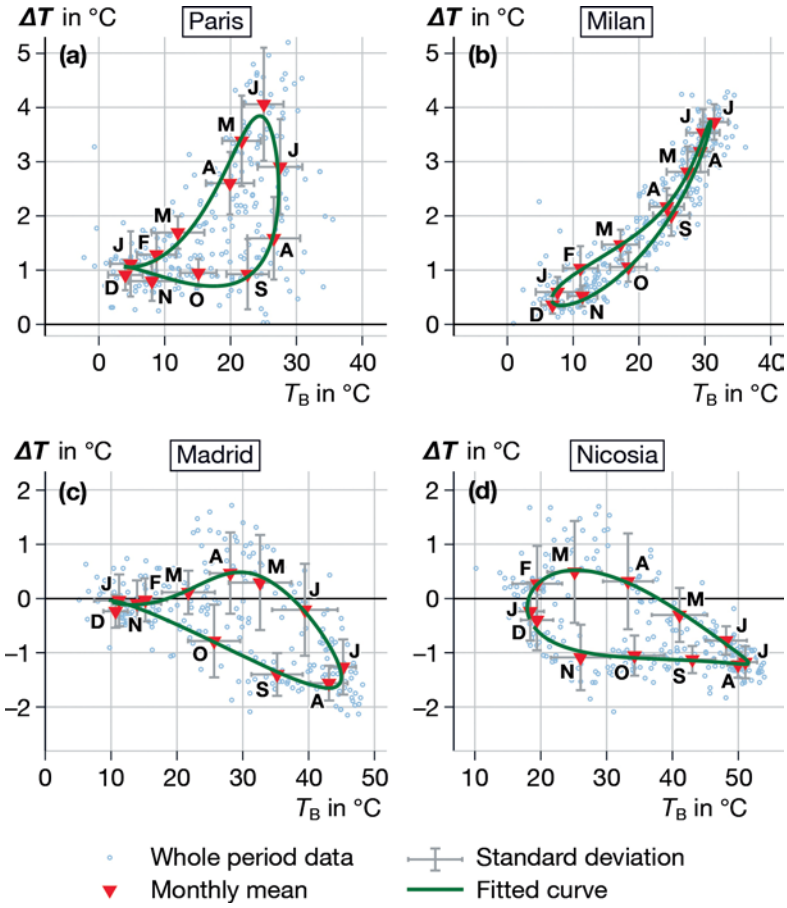

Figure 9: The UHI intensity for different cities plotted versus the temperature outside the city (T_B). The values are drawn as small circles while monthly means are given as red triangles together with the standard deviations (grey error bars) (data: Land Surface Temperatures, LST, 2006–2011, from remote sensing data; validation with in situ measurements indicated an accuracy of < 1 K in most cases; source: Zhou et al. 2013; modified).

The intensity of the UHI and its diurnal variation is determined by extrinsic and intrinsic factors. Extrinsic factors include, for example, the latitude of a city (Wienert and Kuttler, 2005), the proximity to large water bodies (due to the land-sea-breeze effect), the geomorphological location (Ma et al., 2021) and the climate zone (Zhou et al., 2017). Typical intrinsic dependencies are population density (Ma et al., 2021), city structure (ratio of ground plan/surface plan), city size and city shape. The latter was already pointed out by Kratzer (1937) in the context of his qualitative studies for the city of Bremen. Zhou et al. (2017) analysed the quantitative dependence of the surface air UHI intensity on the urban form based on the influencing variables already described in Section 2.1. The result shows that city size has the strongest influence (strong positive correlation) on UHI intensity, ahead of compactness (fractal dimension; positive correlation) and anisometry (negative correlation). Consequently, the creation of large, compact and circular cities should rather be avoided. This was the aim of Kratzer (1937), who pointed out that "linear cities", i.e. cities with short distances to the surrounding countryside and farmland, lead to a more pleasant urban climate for the population due to their "narrowness". Emissions from individual transport might be reduced by sophisticated passenger transport systems. A current example is the "Neom" project planned for the northwest coast of Saudi Arabia, the realization of which is to result in a 170 km long line city ("The Line").

Especially for the planning of fast-growing cities in developing countries, the mentioned findings are likely to be advantageous in order to avoid subsequent negative environmental impacts on the inhabitants.

Other intrinsic factors that affect the UHI include building materials, degree of sealing, level of soil moisture, contribution of anthropogenic heat flux (including night-time lighting), population density (Ma et al., 2021), annual precipitation sum, level of air temperature, and rural soil moisture (details in Manoli et al., 2019, Hupfer and Kuttler, 2006).

As an example, the influence of the rural temperature on the urban boundary layer UHI will be briefly discussed here. Fig. 9 contains examples of Paris, Milan, Madrid and Nicosia. For Paris and Milan, there is a somewhat strong increase in UHI intensity with increasing air temperature. In the case of Madrid and Nicosia, on the other hand, the intensity tends to decrease, especially with very high values of air temperatures. This points to the influence of the oasis effect ($Q_E > Q^*$), whereby it is assumed that evaporation in the two cities

Table 8: Characteristics of the most important properties of different UHI types to be spatially and temporally differentiated (source: Henninger and Weber, 2020).

Properties	**UHI^{SFC}**	**UHI^{UCL}**	**UHI^{UBL}**	**UHI^{SUB}**
Considered quantity	Surface Temperature	Air temperature	Air temperature	Soil and groundwater temperature
Time of maximum UHI				
– Time of Year	Summer	Summer	Summer	Summer
– Time of Day	Middle of day	Middle of night	Middle of night	no or hardly any diurnal fluctuations
Area-sharp demarcation	Yes	No	No (downwind of the city)	No
Typical intensity $\Delta T_{urb-rur}$ (K)	> 10–20 K	1–10 K	1–3 K	1–8 K
Typical identification methods	Satellite, aircraft sensors	Measurement at climate stations, mobile measurements	Vertical soundings, ground-based remote sensing	Stationary measurements
Influencing factors	Physical and thermal properties of the material, increased absorption of short-wave radiation, exposition	increased absorption of short-wave radiation, delayed heat release to nocturnal boundary layer, reduced net longwave loss/reduced effective radiation	turbulent transport of Q_H from the UCL, superimposed wind field determines the thickness	Heat conduction of the materials, thermal properties of urban construction in the subsurface

provides cooling when urban green spaces are irrigated, which does not occur in the dry surrounding countryside where there is a lack of water. In this context, it is also interesting to note the hysteresis effect that develops over the course of the year. The example of Paris shows that at the same ambient temperatures ($t_{rur} \approx 22\,°C$) the UHI values for May ($\Delta T \approx 3.3$ K) and September ($\Delta T \approx 1$ K) differ significantly. This seasonality is because a city with heterogeneous development tends to follow the "astronomical annual cycle" in May when the sun is high in the sky and therefore becomes considerably warmer than the surrounding area, which is characterized by its natural regional climate. This is only the case to a lesser extent in September when the sun is lower (Zhou et al., 2013).

Basically, the following types of urban overheating can be distinguished in different vertical layers (see Table 8; an explanation of the layer designations is given in Chapter 4): the surface heat island (UHI of surfaces), the urban canopy layer heat island (UHI of UCL) and the urban boundary layer heat island (UHI of UBL).

The UHI of surfaces is driven by solar irradiance and surface temperature. Since this type of heat island is controlled by the distribution of built-up/non-built-up areas, it can be obtained from aerial radiometer IR measurements if the ε-values of the materials are known.

The UHI of the urban canopy layer, which refers to the air temperature between the surface and mean roof height (usually measured at 2 m a.g.l.), occurs due to energy release, thermal inertia of building structures, and reduced net longwave radiation due to canyon walls. This type of heat island is only quasi-uniform in its spatial distribution with the built-up area. An example of an extensively formed UHI of the UCL is shown in Fig. 10. The range of mean air temperature differences amounts to about 8 K. The areas with dense development, such as downtown areas are clearly prominent. Cooler areas are obvious in smaller valleys and near larger green areas. Also some "heat cliffs" are evidently characterised by larger horizontal gradients of air temperature. Such heat cliffs are mostly observed where surfaces with thermally very different behaviour (sealed–unsealed) are located next to each other. The temporal variation of the UHI over the year is characterised by a distinct summer maximum occurring during night-time, when heat is released from the urban fabric and net longwave radiation is limited due to the three-dimensional structure of the city (Fig. 11). On average, the UHI in a mid-sized city might reach intensities of about 4 K during summer nights. During daytime hours a slightly cooler urban temperature might evolve ("urban cool island") due to shading of the site by adjacent buildings. However, the strength of the "cool island" effect strongly depends on the structure and exposition of the site surroundings. A guidance on measuring, modelling and monitoring the UHI is documented by Schlünzen et al. (2022).

The UHI of the urban boundary layer is mainly formed due to turbulent heat transport from the UCL. This type of heat island can vertically extend into the atmosphere and is subjected to a downwind drift, i.e.

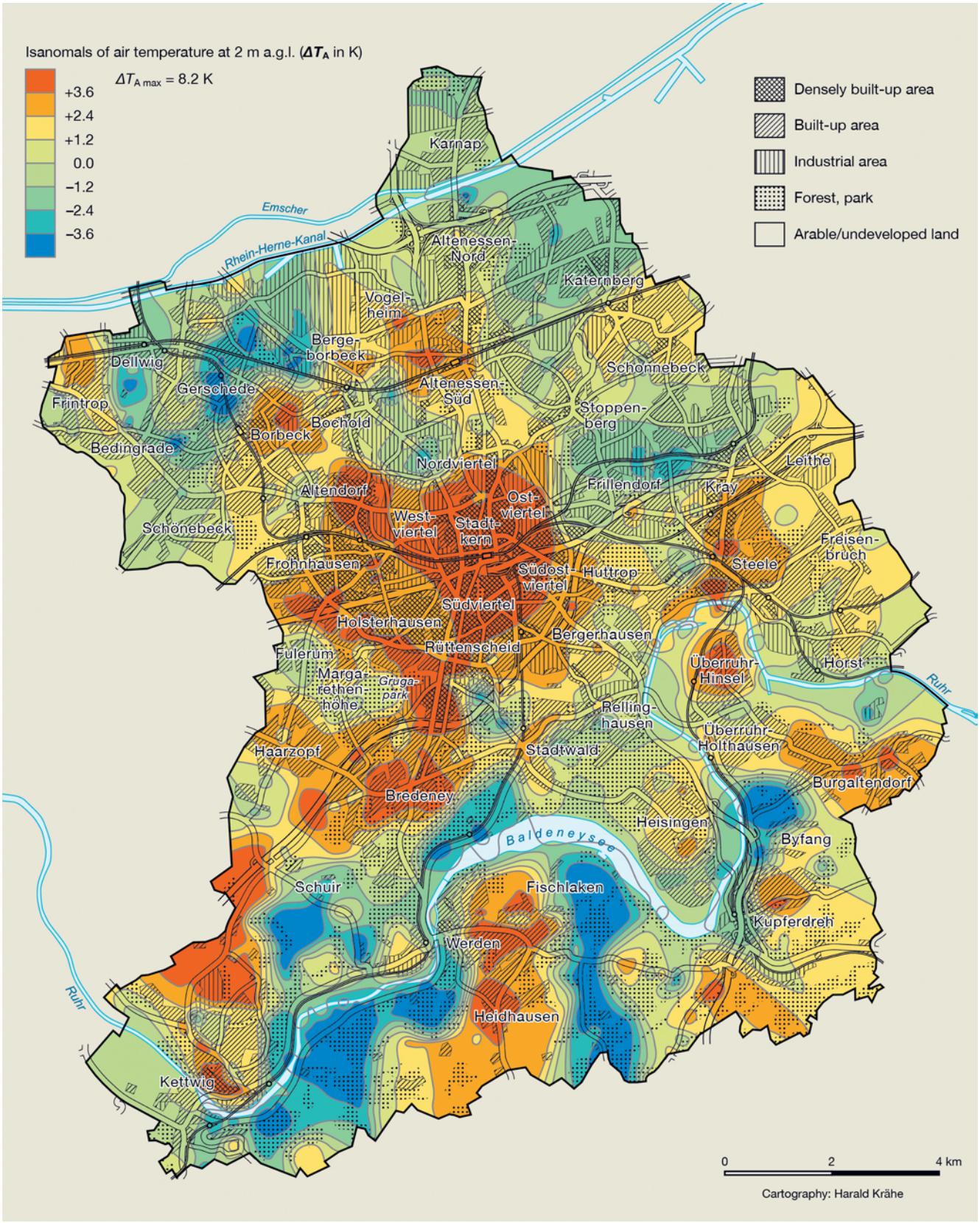

Figure 10: Mean UCL-UHI in Essen, Germany, during nights with weak wind and no clouds (mean of mobile measurements on 23./24.7., 30./31.8., 6./7.9. 2013); source: KUTTLER et al., 2015; modified).

Table 9: Water balance components of sealed surfaces in Berlin (measurement time: 04/1985 to 03/1986) (source: Wessolek, 2001)[1].

	Precipitation		Discharge		Infiltration		Evaporation	
	mm	%	mm	Q_{prec}(%)	mm	Q_{prec} (%)	mm	Q_{prec} (%)
Artificial stone slabs with mosaic paving (sidewalk)	631	100	104	16	319	51	208	33
Composite concrete blocks	631	100	103	16	379	60	149	24
Grass pavers	631	100	32	5	318	50	282	45
Street (asphalt)	631	100	455	72	51	8	126	20

[1] $Q_{\text{prec}} = \frac{\Sigma_{\text{discharge}} \Sigma_{infiltration;} \Sigma_{\text{evaporation}}}{\Sigma_{\text{precipitation}}} \cdot 100\,\%$

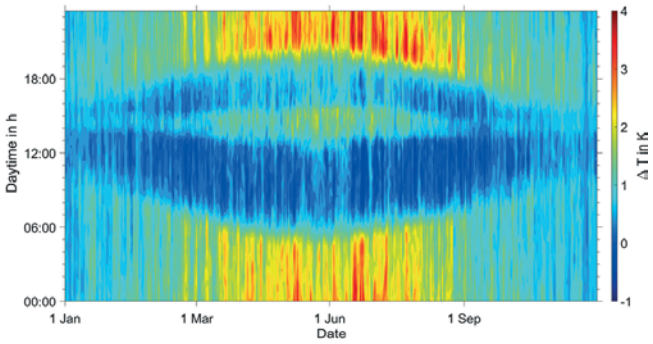

Figure 11: Annual variation of half-hourly average UCL-UHI intensities ($\Delta T_{\text{urb–rur}}$) for Braunschweig, Germany (250,000 inhabitants) covering the time-period 2012–2020. Observations are from a north–south exposed urban street canyon in the centre of Braunschweig and a rural site in the west of the city, details on both sites are given in Grunwald et al. (2019).

the urban plume, by the horizontal flow (urban plume, Chapter 4).

6 Urban water balance

The urban water balance is not just influenced by water input (precipitation) and its output (runoff, evaporation), but also by the hydrological properties of urban surfaces. The latter will be dealt first, before the urban water balance is discussed in more detail.

6.1 Hydrological properties of urban surfaces

The hydrological properties of urban surfaces determine evaporation, runoff, infiltration and capillary rise of soil water. These properties are determined, among other things, by the degree of sealing (λ) and the pore volume of the soil. Surface runoff also depends on the slope and the material-specific wetting capacity w_c. The latter is the amount of water adhering to a particle surface that surrounds it before runoff begins. For example, asphalt (depending on the season) reaches a value of $w_c = 0.3$ mm to $w_c = 0.8$ mm (Wessolek and Facklam, 1997).

To allow water to percolate into the sealed subsoil layers, porous, permeable materials should be used. If this is, however, clogged by clay-rich dust on the surface, the infiltration rate is lower than for permeable openings filled with sand. Exemplary values of the water balance components for different urban surfaces are given in Table 9.

Asphalt surfaces have the highest runoff with > 70 % of the annual precipitation, whereas that of grass pavers (e.g. typical for paved parking lots) is only 5 % on average. With infiltration, however, the ratios are reversed: While only 8 % of the water infiltrates into asphalt surfaces, it is up to 60 % for other materials. With regard to evaporation, only 20 % of the precipitation water is evaporated over asphalt (essentially shortly after previous precipitation), whereas about 45 % is evaporated over grass pavers.

Moreover, urban surfaces can play a prominent role in groundwater recharge because of the heterogeneity of the material. For example, sealing materials with a high proportion of joints and evaporation barrier layers applied to soils (e.g. gravel) have higher groundwater recharge rates (> 50 % of precipitation) than open farmland or woodland. This is of interest, as infiltrating water is more strongly protected against evaporation than uncovered natural surfaces due to the partial sealing of surfaces. This shows that urban areas must be regarded as very differentiated in terms of their groundwater recharge rate.

6.2 Urban water balance

Compared to the surrounding natural countryside, the urban water balance is determined by the city-specific hydrological surface characteristics. Furthermore, the absence of vegetation cover contributes to the fact that less water reaches the atmosphere by plant transpiration and evaporation of interception water. The water cycle is also influenced by the inflow and outflow of water for utility purposes, which enters a city through both water pipes and open canals. In addition, water vapour is transported into the urban atmosphere by industrial processes, cooling tower vapour and motor vehicle emissions. The urban water balance can be written as (after Helbig, 1987; Wessolek et al., 2009, modified):

$$P + Q_R + W_{Fl} - ET(ET_{\text{un}}, E_v, E_0) - \Delta R(Q_v, Q_{\text{un}}, Q_k) - \Delta S\,(V_v, V_{\text{un}}, \Delta S_o) + \Delta A + I = 0 \quad \text{(all in mm (time unit)}^{-1}\text{)} \quad (6.1)$$

With P the precipitation, Q_R the water release through combustion processes, W_{Fl} the water supply from rivers, canals or reservoirs, ET the evapotranspiration, with ET_{un}, the evapotranspiration of unsealed surfaces, E_v and E_0 the evaporation of sealed and water surfaces, respectively, ΔR the net runoff, with Q_v, Q_{un}, Q_k the surface runoff from sealed, unsealed surfaces as well as the surface runoff that is discharged into the sewer system, ΔS the net water storage with V_v, V_{un} the infiltration of sealed and unsealed surface parts, ΔS_o the surface storage, ΔA the net atmospheric moisture advection and finally I the interception (all in mm (time unit)$^{-1}$).

From the individual parameters mentioned here, Q_R is mainly directly influenced by humans, while ET, ΔR and ΔS are rather indirectly anthropogenically controlled via the proportion of sealed area or through surface compaction. The source terms are P, Q_R and W_{Fl}, whereas ET and I are sink terms. The terms ΔR, ΔS and ΔA can assume both source and sink functions. In cities, the share to be spent on irrigation of green may be significant and acts as a source of evaporation.

The terms contained in Eq. (6.1) show that it is difficult to precisely determine the area-related water balance of an urban body, as a great deal of information must be available not only about the use, but also about the small-scale occurrence of the sealing materials (for more information, see Wessolek et al., 2009).

6.2.1 Urban precipitation

Urban precipitation influences are considered to be multicausal, since processes with varying degrees of interaction are involved. However, there are three overriding factors which can play a decisive role in the modification of the precipitation by urban areas. These include (Schütz, 1996; Shepherd, 2005):

- Modified cloud dynamics through the UHI effect and urban surface roughness,
- interference in cloud physical processes by particle emissions from urban-industrial sources, and
- modification of boundary-layer processes by roughness-induced droplet deflection in the near-surface wind field.

Urban overheating, together with the greater surface roughness of the air flowing towards the urban body, leads to a vertical convergence (lifting) and lateral divergence (flowing around) of the urban flow. This can lead to the formation of shallow cumulus clouds, mainly in summer (Inoue and Kumura, 2009). An increase in precipitation can be observed in downtown and urban leeward areas, which suggest, for example, a summer precipitation increase (due to convection) of about 10 % for Tokyo compared to the surrounding area. An accumulation of precipitation events in the afternoon hours dependent on the diurnal cycle was also identified (Seino et al., 2018), confirming former research on urban precipitation. The influence of emitted particles on precipitation depends on their hydrophilic or hydrophobic surface properties.

Finally, surface roughness can lead to a deflection of the falling drops by "combing out" the precipitation over areas with large obstacles (e.g., high buildings) and thus contribute to a more or less effective offset of the falling drops.

It is difficult to determine, which of the mentioned processes primarily influences urban precipitation modification. There is much to suggest that convective processes in particular are intensified by urban excess heat (e.g. Theeuwes et al., 2019), which is also shown by an increase in thunderstorms and heavy rainfall in some urban areas compared to their surroundings (Niyogi et al., 2011).

Slight, but significant differences in the weekly cycle were found in long-term studies in Melbourne, Australia, according to which it rained slightly more on weekdays than on weekends (Simmonds and Keay, 1997).

In recent years, however, it has also been shown that cities not only increase precipitation activity in certain areas, but apparently also lead to a reduction of the precipitation activity depending on the size of the emitted particles (Rosenfeld, 2000). In particular, the release of smaller particles seems to lead to a suppression. Thus, if in a city predominantly smaller particles are emitted into the atmosphere, this is more likely to inhibit nucleation and thus impede the formation of droplets. However, it is still under debate which role ultrafine particles ($Dp < 100$ nm) play in modified rainfall patterns (e.g. Junkermann and Hacker, 2022).

Cities and industrial areas also influence the quality of precipitation water (Table 10). The pH-values in urban areas are clearly below those of the rural locations, while the concentrations and flux rates of anthropogenic pollutants are in some cases significantly higher than in the rural surrounding.

6.2.2 Anthropogenic water vapour release

Anthropogenic water vapour release is defined as the emission from combustion processes of fuels and heating materials within an urban area. The release of water vapour from industrial processes is not taken into account here.

The amount of water release through combustion processes and its share in the total sum of urban water balance varies due to climatic influences, the urban structure and shape, and in particular by the methods used to record the consumption of fuels. For Hong Kong the anthropogenic contribution to urban humidity (vehicle, industrial and power plant emissions) is given as 38 %. The reasons for this relatively high amount can be attributed to the low wind speed – caused by the numerous high-rise buildings – resulting in a decrease in atmospheric exchange (Wang et al., 2020). Boxes 6.1 and 6.2 contain example estimates of anthropogenic water vapour emissions resulting from the combustion of fuel by vehicles and gas consumption.

Table 10: Chemical composition and flux rates of wet deposition for urban and peri-urban sites in South Africa (source: Conradie et al., 2016). EC, pH and ionic concentrations are specified in µEq L^{-1}; flux rates are given in kg ha^{-1} a^{-1} of wet deposition.)

	Industry / Urban[1]		Industry / Urban[2]		Rural[3]		Rural[4]	
	VWM values[5]	Fluxes	VWM values	Fluxes	VWM values	Fluxes	VWM values	Fluxes
pH	4.32		4.51		4.89		4.66	
EC	42.60		33.60		13.10		22.90	
H^+	61.18	0.45	44.64	0.43	15.24	0.11	22.24	0.13
Na^+	17.79	2.98	3.50	0.77	7.75	1.30	13.17	1.77
NH_4^+	28.50	3.75	29.06	5.01	10.85	1.42	12.80	1.35
K^+	7.35	2.10	1.41	0.53	5.12	1.46	2.08	0.48
Mg^{2+}	5.54	0.49	4.55	0.53	1.93	0.17	3.27	0.23
Ca_2^+	16.39	2.40	16.18	3.10	6.25	0.91	4.69	0.55
NO_3	33.40	15.11	22.97	13.62	7.49	3.38	13.20	4.77
Cl^-	17.96	4.65	4.52	1.53	10.83	2.80	15.23	3.25
SO_4^{2-}	67.21	23.56	55.00	25.27	12.37	4.33	18.66	5.23

1) Amersfoort; 2) Vaal Triangle; 3) Louis Trichardt; 4) Skukuza; 5) Volume Weighted mean (VWM)

Box 6.1: Estimation of water vapour emissions from motor vehicles in a large city at mid-latitudes.

	Based on	Assumptions[1),2)]	Data
1	City	Essen, Germany	Area: 210 km^2
2	Vehicles	Number of daily vehicle movements (estimated)	2×10^5
3	Driven route	Per vehicle	20 km d^{-1}
4	Average fuel consumption	For all vehicle types	8 L (100 km)$^{-1}$
5	Chemical equation	Petrol = Octane	$2\,C_8H_{18} + 25\,O_2 \rightarrow 16\,CO_2 + 18\,H_2O$
6	Combustion of 1 kg octane yields 1.3 kg water	–	$1\,kg_O = 1{,}3\,kg_W$

Taking into account 2), 3) and 4), this results in: 336 m^3 water d^{-1}
Converted to the urban area and the year, this results in an average value of 0.6 mm a^{-1} (condensed water) and, with reference to Q_E = 0.39 kWh m^{-2} a^{-1}
1) No advection and constant traffic density.
2) Average density of petrol/diesel ρ = 750 kg m^{-3}

Box 6.2: Estimation of water vapour release from natural gas combustion in a large city (only buildings).

	Based on	Assumptions[1)]	Data
1	City	Essen, Germany	Area: 210 km^2
2	Average yearly gas consumption (Methane)	City of Essen, 2021	3000 GWh a^{-1}
3	Calorific value (Methane) H_s	–	10 kWh m^{-3}
4	Chemical equation	Natural gas = Methane[2)]	$CH_4 + 2\,O_2 \rightarrow CO_2 + 2\,H_2O$
5	Combustion of 1 kg methane yields 2.3 kg water	–	$1\,kg_M = 2{,}3\,kg_W$

Taking 2)–5) into account, this results in $5.2 \cdot 10^5$ m^3 water a^{-1}
Converted to the urban area and the year, this results in an average value of 2.5 mm a^{-1} and, with reference to Q_E = 1.7 kWh m^{-2} a^{-1}
1) No advection, consumption data according to City of Essen 2021 (Environmental Agency).
2) Gas density ρ_{Gas} = 0.75 kg m^{-3}

6.2.3 Urban evapotranspiration

Evapotranspiration in urban areas is generally severely limited due to the high fraction of sealed surfaces (cf. Section 5). It is only possible immediately after wetting by precipitation ("interception water" of natural and artificial surfaces), via open water surfaces, and transpiration of vegetation.

It is difficult to compare data on urban *ET*; because different measurement methods are used (e.g. microlysimeters, eddy covariance, theoretical calculation methods, see e.g. Harlass, 2008), and the scales of the catchment areas as well as detailed land use and their water supply are rarely given. Furthermore, the amount of urban *ET* is also influenced by irrigation of gardens and lawns, by swimming pools as well as the spraying of streets with water for cooling during particularly hot weather. The latter process is known in Japan as traditional "uchimizu" (for details see Solcerova, 2018).

The eddy-covariance method, for example, is a suitable means of measuring actual *ET* in cities with high

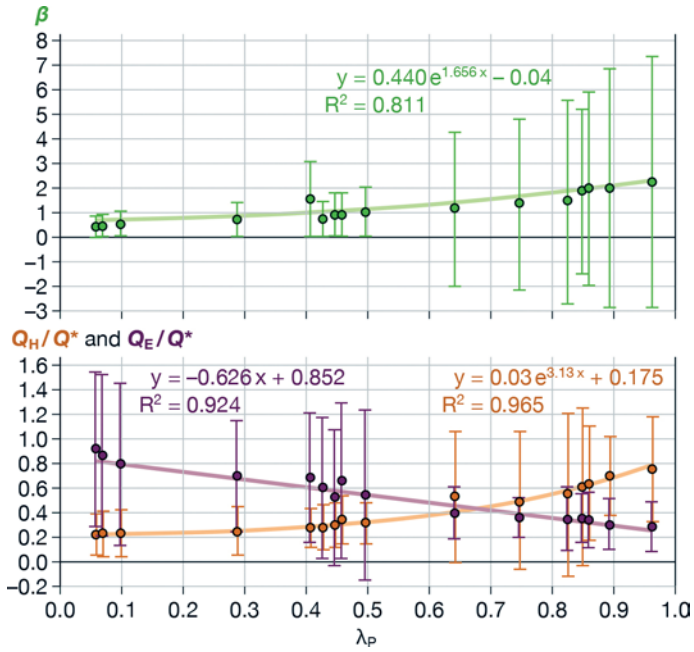

Figure 12: Average Bowen ratios (β) and partition of the turbulent heat flux densities (Q_H/Q^*, Q_E/Q^*) as a function of the plan area fraction (λ_b) ($Q^* > 0\,\mathrm{W\,m^{-2}}$~; error bars are $\pm 1\sigma$) (measurement sites in Oberhausen, Germany; source: Goldbach and Kuttler, 2012).

temporal resolution (Vulova et al., 2021). This can be used to record the turbulent water vapour exchange with high frequency (≥ 10 Hz) on flux towers, which should usually have at least twice the height of the roughness elements and are representative for the so-called flux footprint of about 10^2–10^4 m horizontal length scale. Since evapotranspiration links the energy balance with the water balance, evapotranspiration totals per time and area fraction can be derived from it.

Direct measurements at two sites in Berlin, Germany, using the eddy-covariance method demonstrate an *ET* amount of 366 mm a^{-1}, which is higher by a factor of 1.6 at the more vegetated site (measurement height at 39.75 m above ground level, 51 % vegetation areas in the flux footprint) compared to the less vegetated site (measurement height at 56 m above ground level, 33 % vegetation area share). Hence, eddy-covariance sensors at both flux towers were placed within the inertial sublayer allowing for representative observations of surface–atmosphere exchange of water vapour from the flux footprints (cf. Fig. 3). With regard to the potential of green infrastructure in municipal climate adaptation measures, the improved quantification of the *ET* performance of different vegetation areas or types will play an increasingly important role. For extensive green roofs, for example, it has been shown that energy is mainly partitioned into latent heat if there is sufficient precipitation, and that evaporation rates between 228 and 303 mm a^{-1} can be achieved (Konopka et al., 2021). However, the performance of an extensive green roof with low substrate thicknesses (< 0.1 m) is strongly dependent on the meteorological boundary conditions, as precipitation-free episodes lead to drying out of the substrate relatively quickly (Heusinger and Weber, 2017).

Fig. 12 shows how strongly the building plan area fraction (λ_b) determines the value of the Bowen-ratio (β) and the latent heat flux (*ET*). The Q_E/Q^* ratio decreases significantly with increasing λ_b. While, for example, with a surface area of 10 % building coverage, about 80 % of the radiation balance is partitioned into evapotranspiration, this is only 30 % with a λ_b value of 0.9. The specification of the respective standard deviations shows that the fluctuation range of the *ET* value is on the one hand relatively large with a low λ_b. The clear decrease in the standard deviations with increasing λ_b-values, on the other hand, shows the influence of the built-up area on reduced evaporation.

6.2.4 Humidity, fog and dew

Humidity

The mean humidity values of urban and urban forest areas in a mid-latitude city (*rH, e*) differ only slightly from each other (Table 11).

Table 11: Yearly means of relative humidity (*rH*) and water vapour pressure (*e*) for urban and urban forest areas (mainly deciduous trees, forest area: 10 ha) in Essen, Germany[1)] (source: Kuttler et al., 2015; N = number of observations).

	Urban			Urban forest		
	Mean	**Min, abs.**	**Max, abs.**	**Mean**	**Min, abs.**	**Max, abs.**
***rH* in %**	71	18	100	79	22	100
***e* in hPa**	9.7	1.5	23.8	10.1	1.6	24.5

[1)] 6/2012–5/2013; $N_{urb} = 15$, $N_{urbforest} = 2$

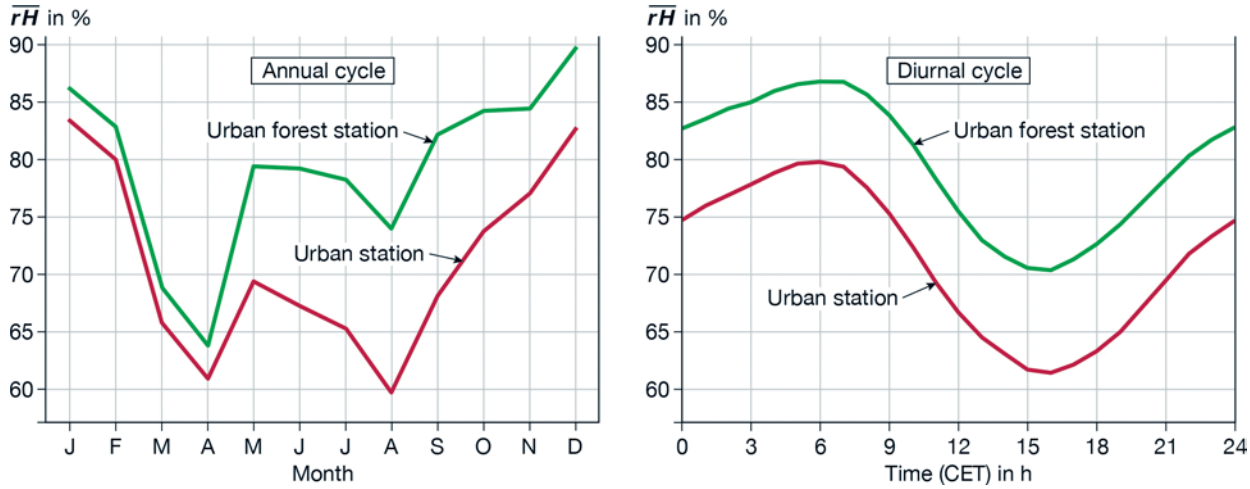

Figure 13: Annual (left) and daily (right) variations of relative humidity (*rH*) for an urban and an urban forest area (mainly deciduous trees, forest area: 10 ha) in Essen, Germany (07/2012–09/2013; source: Kuttler et al., 2015; modified).

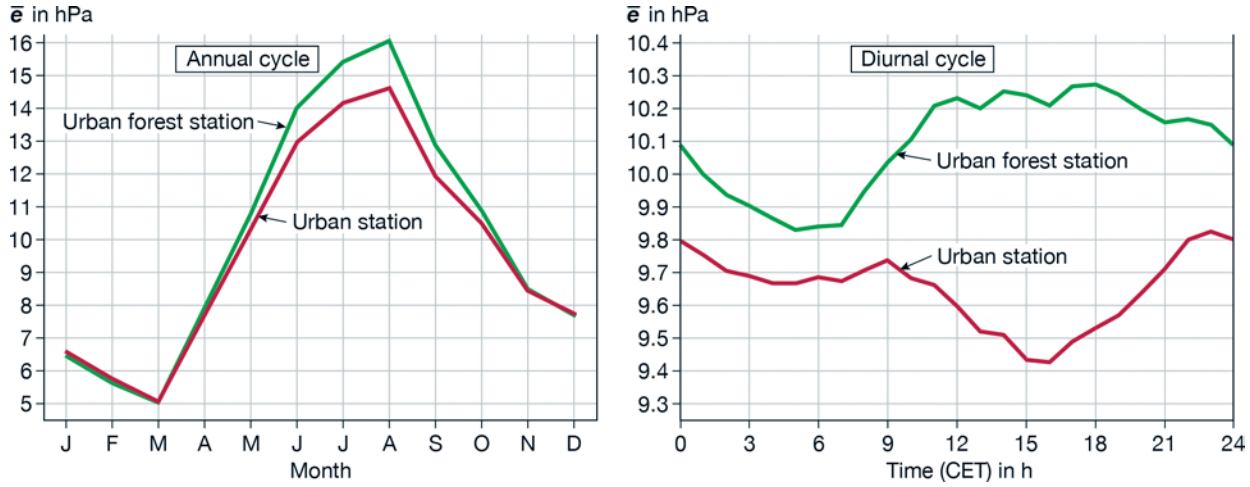

Figure 14: Annual (left) and daily (right) variations of mean vapour pressure (*e*) for an urban and urban forest area (mainly deciduous trees, forest area: 10 ha) in Essen, Germany (07/2012–09/2013; source: Kuttler et al., 2015; modified).

Thus, the annual mean values in the urban forest are only slightly higher than in the city centre. In the annual and diurnal variation, however, there are greater differences in relation to the two sites mentioned (Fig. 13).

The annual cycle for *rH* is characterized by two minima in spring (April) and summer (August), which may refer to a general lack of precipitation. As expected, the highest values are evident in the winter months. During all months of the year, the highly sealed inner-city station is the driest. The urban forest site, on the other hand, has the highest values in each case, whereby the differences to the inner city are highest with almost 15 % *rH*, especially in summer months. In the mean diurnal variation of *rH*, clear differences between the land-use emerge. At the inner-city station, the lowest humidity values are reached in the early afternoon whereas values of the forest station are comparable to those of the city during the course of the day but reach a significantly higher level. The higher forest station values are probably due to transpiration, and the lower air exchange caused by the canopy density.

The course of *e* shown in Fig. 14 (left) is characterized by a pronounced mean annual cycle for both sites. Remarkable differences between the vapour pressure values of both sites can only be seen in the summer months, with up to $\Delta e_{\mathrm{urb-rur}} \approx 1.5$ hPa.

On the diurnal cycle (Fig. 14 (right)), lowest values are reached before or around sunrise both in the city and in the urban forest. Afterwards, the values increase at both sites, but in the city forest much more strongly and remaining at a high level throughout the day until the evening ($e_{\mathrm{rur}} > 10$ hPa), while in the city centre the vapour pressure drops to a minimum until the afternoon and increases again towards evening. The minimum at the urban site is due to increased turbulence, especially in the afternoon. At the urban forest site, the vapour pressure values remain at a relatively high level because the canopy limits vertical exchange. This is supported by a summer/winter comparison of the vapour pressure values (not shown here), whose differences between the two sites are considerably higher in the

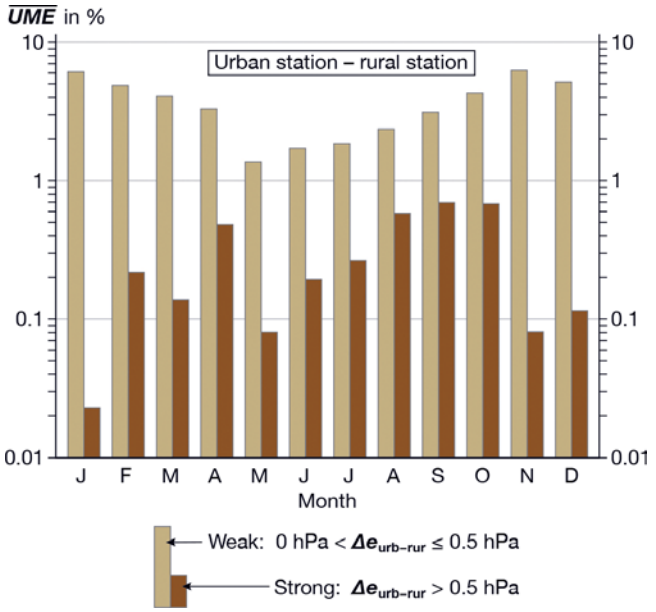

Figure 15: Average hourly urban excess humidity (UME; in % of annual hours) based on an inner city and surrounding area station for weak ($0\,\text{hPa} < \Delta e_{\text{urb–rur}} \leq 0.5\,\text{hPa}$) and strong ($\Delta e_{\text{urb–rur}} > 0.5\,\text{hPa}$) UME events in Essen, Germany (06/2012–05/2013; source: Kuttler et al., 2015, modified).

summer afternoon ($\Delta e_{\text{urb–rur}} > 2.0\,\text{hPa}$) than in winter ($\Delta e_{\text{urb–rur}} < 1.0\,\text{hPa}$).

Apart from the average humidity conditions between the city centre and the urban forest, weather situations are evident during which the humidity conditions in the city are higher than in the rural area ($\Delta e_{\text{urb–rur}} > 0\,\text{hPa}$), i.e., Urban Moisture Excess (UME or UMI, Urban Moisture Island, see Richards, 2005; Kuttler et al., 2007). The reason for the higher urban humidity at this specific observation site, which is particularly pronounced in the second half of the night, is probably because in the surrounding boundary layer the dew point temperature is reached earlier in the evening and more frequently at night due to the stronger cooling of the rural boundary layer. Another reason is longer-lasting *ET* in the warmer UBL compared to the cooler surrounding area. Limited influence on UME is related to the anthropogenic emission of water vapour (motor vehicle traffic, industry, cooling towers) and to a lower frequency and sum of dewfall on green roofs ($x_{\text{green roofs}} = 0.3\,\text{mm month}^{-1}$) in comparison to bitumen roofs ($x_{\text{bitumen roofsr}} = 0.4\,\text{mm month}^{-1}$ in each case without fog events; Heusinger and Weber, 2015).

Fig. 15 shows an example of the relative frequency of weak UME events ($0\,\text{hPa} < \Delta e_{\text{urb–rur}} \leq 0.5\,\text{hPa}$) and strong UME events ($\Delta e_{\text{urb–rur}} > 0.5\,\text{hPa}$) on the annual cycle. Strong UME events occur – although in small absolute numbers and except for the winter months – during all seasons. The frequency of occurrence is < 1 %. Weak UME events, on the other hand, have frequencies of up to 5 %. Most UME events last only a few hours (87 % ≤ 5 hours, for further details refer to Kuttler et al., 2015).

Analyses of long-term trends in urban humidity indicate statistically significant decrease for rapidly expanding cities. For example, an analysis conducted for Beijing, China (1961–2014) showed a decrease in e (−0.24 hPa/decade.), specific humidity (−0.15 g/kg/decade.) and an increase in vapour pressure deficit of 0.14 hPa/decade. These changes are related to the increase in sealed areas of the respective cities (Li et al., 2021).

Fog

Analyses of urban and rural fog frequency indicate a turnaround of the situation in recent decades indicating that it is no longer that the urban area has the greater number of fog days, but the rural area. This antagonistic behaviour compared to earlier studies (until about the middle of the 20$^{\text{th}}$ century) is attributed to the warming of the urban atmosphere and the reduced concentration of fog-producing particles due to air pollution control measures. Studies of large cities in western and southern Germany, for example, show a decrease in urban fog frequency by up to 60 % between 1960 and 2015 (e.g., Kuttler et al., 2015). Comparative measurements between the city of Belgrade (Serbia) and the surrounding area showed that only about two-thirds of the fog days in the surrounding area occurred in the city (Vujović and Todorović, 2018). The decrease in fog frequency for Los Angeles during recent decades is attributed partly to increasing nocturnal minimum temperatures (Williams et al., 2015). A decrease in fog frequency favours traffic safety and increases energy yield of photovoltaic panels. Disadvantages for cities in arid areas, however, are the increased water and energy consumption due to the lack of wetting by deposited fog and higher frequency of sunshine.

Occasionally, during high-pressure "foggy weather conditions", satellite images show cities as fog-free and thus sunny islands surrounded by fog ("Urban Clear Islands", UCI; Lee, 1987; Sachweh and Köpke, 1995). Stronger radiation absorption and the associated warming of the urban surfaces compared to the surrounding area ensure an increase in midday thermal turbulence and atmospheric instability. This leads to increased downward transport of warm and dry air from aloft, reducing near-surface *rH* in the urban atmosphere.

If such weather situations are not isolated, but the urban fog-free conditions last for a longer period, this should also be of human-biometeorological interest, e.g. much more pleasant urban meteorological conditions than in the cold and wet surrounding countryside.

Dew

Dew deposition during periods without rain can have various reasons (Monteith, 1957; Groh et al., 2018) such as (1) the deposition of atmospheric water when the air temperature is equal to or lower than the dew point temperature ($t_a \leq t_d$), (2) the vapour pressure of moist

soil is higher than that of the atmosphere ($e_{soil} > e_{air}$; distillation) and (3) when there is active transport of water from inside the plant body by hydathodes (guttation). The main pathway of urban dew deposition is due to the first reason, if a negative radiation balance, sufficient atmospheric water vapour and low wind speeds occur. An increase in dew deposition can be observed with increasing ψ_{sky} (Richards and Oke, 2002). Mean nocturnal dew deposition rates in Paris reached values of around 0.05 mm night^{-1}. Generally, due to urban warming dew deposition is occurring less frequently than outside the city. Urban dew not only has thermodynamic effects, for example on the duration and strength of the UHI, but also can increase the deposition velocity (v_d) of various air pollutants due to the moist surfaces (Mulawa et al., 1986). Additionally, to evaporate nocturnal dew, about 8 % of the available energy (i.e., Q^*) is needed in summer (southern England, Hughes and Brimblecombe, 1994).

7 Air pollutants

Most of the worldwide emission of anthropogenic trace gases originates from cities. Cities cover less than 1 % of the Earth's surface (Schneider et al., 2009), but are home to about 60 % of world's population. Cities are not only hot spots with regard to the release of air pollutants, but also with regard to the emission of greenhouse gases (e.g., CO_{2eq}.). However, in Europe, emissions of the most important air pollutants have significantly decreased in recent decades, e.g. SO_2 – 80 %, CO – 49 %, NO_x – 46 %, NMVOC – 44 %, $PM_{2.5}$ – 31 %, PM_{10} – 29 %, NH_3 – 10 % (for the time period 2000–2017). The secondary pollutant ozone, however, is characterised by a concentration increase in most European cities and often exceeds the EU limit value (Sicard et al., 2021).

Urban air quality is mainly characterised by gaseous and particulate emissions from near-surface sources such as motor vehicle traffic, domestic heating, and industry. In addition, during hot and low wind summer days, certain tree species (especially Platanus × acerifolia) can locally enhance ozone production through increased emission of the precursor gas isoprene (Simon et al., 2019; Wagner and Kuttler, 2014). In winter, urban air quality can be impacted by PM_{10} emission due to wood combustion in domestic fireplaces (e.g. Küpper et al., 2018).

In addition to gaseous pollutants such as NO, CO, NO_2, volatile organic compounds (VOC) and O_3, particulate matter (PM_{10}, $PM_{2.5}$) plays an important role in the assessment of (urban) air quality. The level of ambient concentrations depends not only on the type of land use, but also on atmospheric stability.

Table 12 contains exemplary annual mean values for urban background, traffic and forest stations of the Rhine–Ruhr conurbation, Germany, which is one of the largest agglomerations in Europe. Urban background areas are characterised by high ozone concentrations followed by NO_2 and PM_{10}. Air quality at traffic stations is dominated by PM_{10} and NO_2. At forest stations, ozone values occur with by far the highest concentrations. The clearest difference between traffic and urban background stations is evident for NO, which is twice as high at traffic stations as in the urban background. In the surrounding area, NO hardly plays a role.

Table 12: Air pollutants in the Rhine–Ruhr Area (Germany) (hourly means in µg m^{-3}; (. . .) = 98 % percentile; based on 2020 (yearly means) except for PM_{10} (year 2018); source: LANUV, 2021, pers. communication).

	Station type		
Pollutant	**Traffic**	**Urban Background**	**Forest**
SO_2	–	6 (40)	–
NO_2	26 (64)	19 (54)	4 (17)
NO	12 (68)	6 (60)	0 (1)
O_3	–	47 (123)	67 (129)
PM_{10}	29	25	12

Street canyons in a city can represent "hot spots" in terms of air quality. It is important to learn, which are the most relevant drivers for high pollutant concentrations in street canyons. A statistical modelling study indicates functional relationships between street canyon NO_2 concentrations (as an example) and explanatory variables (for method cp. van Pinxteren et al., 2021) (Fig. 16).

The hour of the day has the largest influence on the NO_2 concentration with >45 % and is mainly attributed to the time-dependent traffic rate (e.g., emission of precursor gases during morning and evening rush hour). The second most important influence is from wind speed especially at low values with $v \leq 1$ m s^{-1}. The mean influence of the day of the week is 12.2 %. There is hardly any difference between the weekdays, but a relatively strong reduction towards the weekend, especially towards Sunday. In the annual cycle (4.1 %), the winter months show higher concentrations. Air temperature shows a U-shaped relationship with NO_2 increase at very low but also very high temperatures. The influence of very low air temperatures is likely to be due to increased engine emissions from warm-up phases (Suarez-Bertoa and Astorga, 2018), while that of high air temperatures should be related to ozone chemistry.

The influence of rH (2.5 %) is interesting: drier air results in higher NO_2 concentrations. This decrease in concentration with an increase in humidity (and dewfall at night) is probably also related to the fact that v_d of air components over moist surfaces increases.

While global radiation and the precipitation amount hardly affect NO_2 concentrations, the trajectory lengths or air mass histories is influencing on relatively short distances (≤ 1,500 m) illustrating a regional impact on the occurrence of higher NO_2 concentrations.

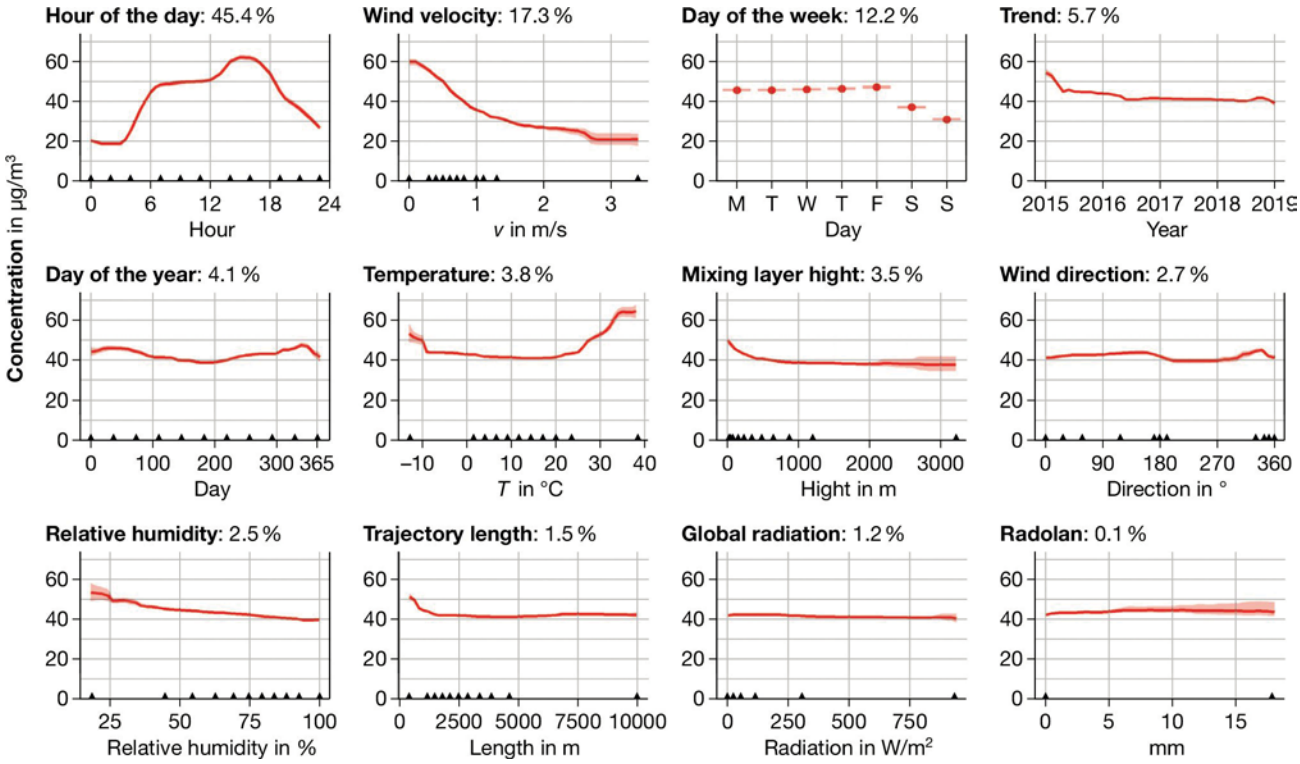

Figure 16: Factors which determine mean NO_2-concentrations at a traffic station sorted by importance (RADOLAN = Radar-Online-Aneichung values). Short vertical lines indicate the value distribution of the variables in 10th percentiles (0 %–100 %) (based on partial dependence plots; Dresden, Bergstraße, 2015–2018; source: VAN PINXTEREN et al., 2021).

Diurnal patterns of selected air pollutants

Over the diurnal course, the concentrations of air pollutants can vary greatly for different reasons (emission strength, atmospheric mixing). The varying proportion of sealed surfaces in cities alone has an effect on the distribution of air pollutants. For example, with a locally high degree of sealing and strong solar radiation, increased turbulence leads to a decrease in the air pollution concentration (larger mixing layer height), whereas higher pollutant concentrations occur in the evening when mixing decreases and the UBL height is limited (FALLMANN et al., 2021). Examples of the behaviour of trace substances of a traffic and rural station are shown in Fig. 17. NO shows a local maximum at the time of the morning rush hour and a secondary maximum during the afternoon rush hour (Fig. 17a). The rural concentrations are not only much lower, up to 75 % of the maximum value measured at the traffic station, but also show little diurnal variation. However, the urban traffic peaks in the morning and late afternoon/evening show slightly higher values also at the rural site with a slight time shift.

The mean diurnal variation of NO_2 (Fig. 17b) shows a similar spatio-temporal behaviour as NO. It is striking that at both locations maximum values do not occur only in the morning, but also between 18 and 20 h. These maxima are probably caused not only by the NO_2 emission from road traffic (as primary emission), but also by the high ozone concentration during the day (Fig. 17c), which acts together with NO as a NO_2 source. In addition, UV radiation decreases towards evening, which reduces the photolysis of NO_2, allowing the pollutant to maintain its elevated concentration. The latter is indicated by the relatively high values towards evening compared to early morning.

The mean diurnal variation of ozone concentration shows an opposite trend to that of NO_x ($NO + NO_2$; Fig. 17c). As a secondary trace gas, ozone is formed from various precursor gases (NO_x, anthropogenic- and biogenic -VOC, PAN, etc.), especially with solar irradiation, so that with increasing solar radiation the near-surface ozone concentration reaches its maximum from midday onwards. At night, the ozone concentrations drop and reach a minimum early in the morning. However, secondary maxima can occasionally be detected at night (1–3 h), which can be attributed to ozone formed during the day. This usually originates from the residual layer above the surface inversion and is transported towards the ground surface by turbulence caused by wind shear (REITEBUCH et al., 1998).

The mean diurnal variation of the PM_{10} concentration shows maximum concentration values at both the inner city traffic and the industrial area station with morning maxima coinciding with the traffic peak (Fig. 17d). Towards evening (> 21 h), another maximum develops, which is slightly below the primary morning maximum at both sites.

However, PM_{10} does not represent the number concentration of all particles, e.g., those of ultrafine particles (UFP ≤ 100 nm), as they have a very small share

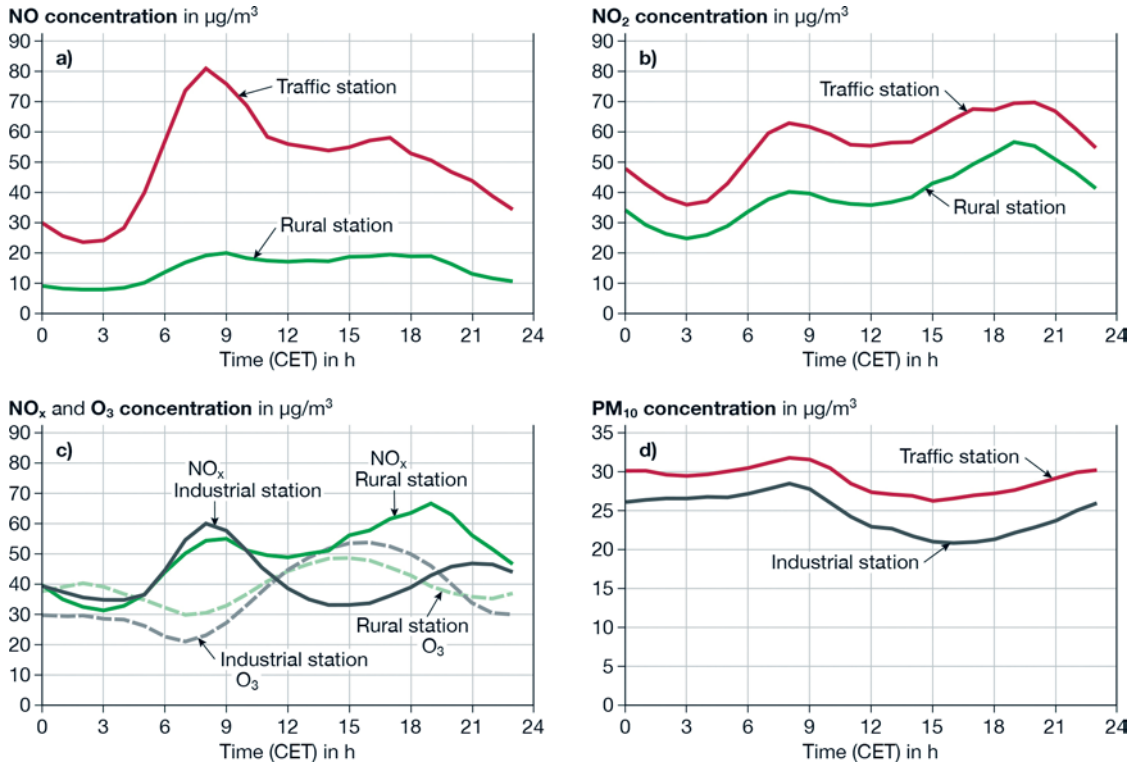

Figure 17: Mean hourly average values of selected air pollutants at different observation sites (traffic, rural, and industrial site) in the area of Essen, Germany (06/12–05/13) (source: Kuttler et al., 2015; modified).

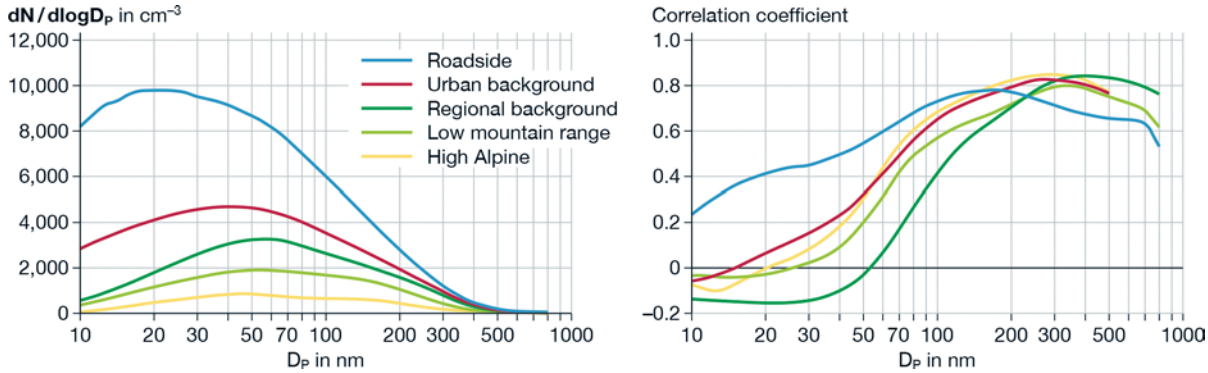

Figure 18: Particle Number Size Distribution (PNSD, left) and correlation between PNSD and eBC (equivalent Black Carbon) Mass concentration (right) for different measurement sites in Germany (hourly means 2009–2014) (source: Su et al., 2019; modified).

of the total particle mass. UFP have a relatively large surface-to-mass ratio. This allows them to more effectively absorb (toxic) substances than larger particles. Because of their small size, UFP penetrate deeper into the human lungs and can be absorbed into the bloodstream, causing respiratory and cardiac diseases. Since UFP show a high affinity to road traffic as a dominant source in cities, concentrations at stations close to traffic can be significantly elevated compared to urban background stations, e.g. by a factor of 1.4 in Leipzig or >3 in London (von Bismarck-Osten et al., 2013). It is interesting to note that despite the site-dependent variability of the number concentrations, a more homogeneous distribution develops towards larger particle diameters (Fig. 18). This "particle ageing" is associated with particle growth, which is attributed to condensation/coagulation, among other factors (Sun et al., 2019).

Evidence that increased concentrations of UFP in the road sector are mainly caused by traffic emissions can be obtained via correlation with eBC (equivalent black carbon: BC + EC), as "soot" is a reliable tracer for traffic emissions (Grange et al., 2020). This correlation is significantly higher in the road area than at the comparison stations (Fig. 18 right), thus proving that UFP are mainly released by motor vehicle traffic.

Greenhouse gases

Cities are not only sources of air pollution but also 'hot spots' of greenhouse gas emission (e.g. $CO_{2eq.}$). Even

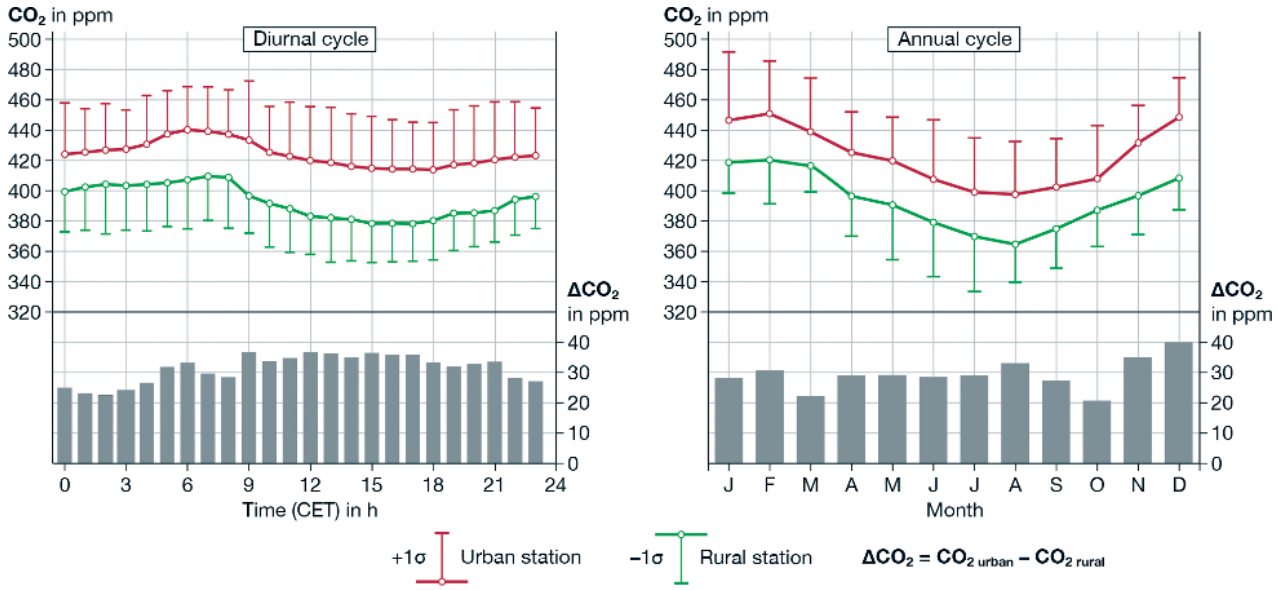

Figure 19: Average diurnal and annual variation of the CO_2-mixing ratio in the city centre and surrounding area station as well as the absolute differences of the CO_2 mean values (ΔCO_2) between both locations in Essen, Germany (06/2012–05/2013; source: KUTTLER et al., 2015).

Table 16: CO_2 emissions of various European cities (source: JASEK-KAMINSKA et al., 2020; based on WARD et al., 2015).

Location	Emission in kg CO_2 m^{-2} a^{-1}
London	35.5
Florence	30.3
Krakow	22.3
Basel	17.6–19.4
Helsinki	17.4
Copenhagen	12.8
Lodz	10.8
Essen	6.0
Gliwice	2.8

though during the summer months urban vegetation can take up atmospheric CO_2 by photosynthesis, in the annual balance the urban CO_2 flux remains positive, i.e. directed into the atmosphere. Depending on the economic structure, population density, degree of green cover and proportion of natural soil, the mean amount of urban CO_2 emissions (F_{CO2}) for selected European cities is in the order of $2\,\mu mol\,m^{-2}\,s^{-1} < F_{CO2} > 25\,\mu mol\,m^{-2}\,s^{-1}$ or between $< 3\,kg\,CO_2\,m^{-2}\,a^{-1}$ (Gliwice, Poland) and $35\,kg\,CO_2\,m^{-2}\,a^{-1}$ (London, UK, Table 13). For estimation of respiratory carbon dioxide of urban dwellers, see (Box 7.1).

Daily and annual variations in CO_2 concentration

Under Central European climatic and economic conditions, urban and rural CO_2-concentrations show almost sinusoidal patterns in the diurnal and annual cycles (Fig. 19). In the diurnal cycle, the maxima with different absolute concentrations at both locations are reached during the early morning hours (rush hour, stable stratification). Subsequently, the values drop to a minimum during the midday and afternoon hours (stronger convection, photosynthesis), only to increase again towards evening (more stable stratification, respiration of the plants). For the example presented here, the daily mean values in the UBL are higher by > 30 ppm than in the surrounding area.

In the annual cycle, the highest CO_2-concentrations for both sites occur in the winter months when photosynthesis is limited, while the minima can be found during the summer months. The higher standard deviations at the urban location are due to the temporal variation in urban emission strength from different anthropogenic sources.

This significant diurnal and annual variation in cities and their surroundings in the mid-latitudes, as described above, is also subject to macroclimatic conditions. Gradual differences are e.g. recognizable in the cities of typical monsoon areas in Asia (Seoul, Korea), where the summer monsoon reduces photosynthesis due to prevailing heavy cloud cover and thus increases the CO_2 concentration during this time of year (HONG et al., 2019).

Box 7.1: Box 7.1 Mean CO_2-emission rate from respiration by city dwellers

An estimate of the fraction of CO_2 released solely by the respiration of urban dwellers, assuming an average person weight of 70 kg, yields an average CO_2 emission of $330\,kg\,CO_2\,cap^{-1}\,a^{-1}$ (PRAIRIE and DURARTE, 2007). If this value is taken as an example for a large city at mid-latitudes (Essen, Germany, 590,000 inhabitants, $A = 210\,km^2$, mean urban anthropogenic CO_2 emission: $6\,kg\,CO_2\,m^{-2}\,a^{-1}$; reference year: 2020), the CO_2 share caused by the inhabitants amounts to about 15 % of the total anthropogenic CO_2 emission in the urban area.

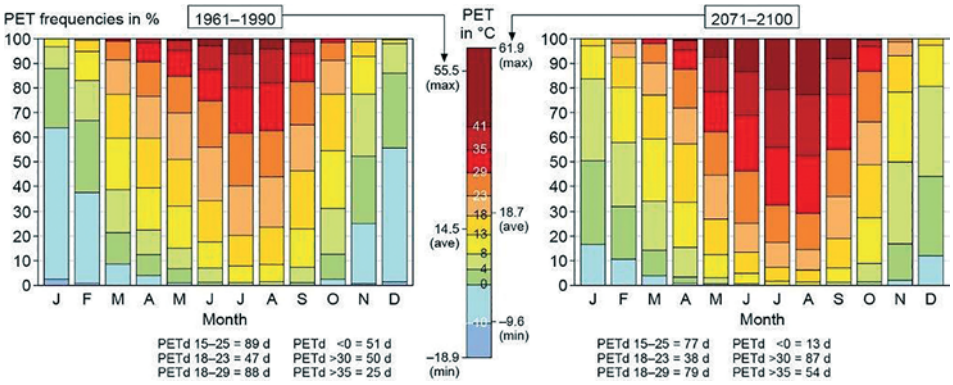

Figure 20: Heat load (Physiologically Equivalent Temperature, PET; PET_d = PET class in days) in Freiburg/Brsg. (Germany) for the periods 1961–1990 and 2071–2100 (PET d 18–29 = thermal acceptable) (source: Matzarakis and Endler, 2010; modified).

With regard to the release of anthropogenic greenhouse gases (GHG) in addition to CO_2, emissions of CH_4 (e.g., from sewage treatment plants, oil refineries and landfills) should be mentioned in particular, which lead to concentrations several times higher in cities than in the surrounding areas (Takano and Ueyama, 2021). GHG footprint analyses that took into account not only CO_2 and CH_4 but also N_2O resulted in the following emission values for Delhi 1.9, Mexico City 3.1, Berlin 8.9 and New York 14.2 (each in $t\ CO_{2eq}\ cap^{-1}\ a^{-1}$; Pichler et al., 2017).

8 Human-Biometeorology

The previous chapters have pointed to distinct spatio-temporal variability of different microclimatic conditions within cities. The extent to which microscale variability of atmospheric conditions can affect human well-being is investigated in more detail in the research field of human biometeorology (e.g. Holst and Mayer, 2011). Depending on the individual physical condition of a person or the state of activity (rest, sporting activity), the human organism reacts differently to meteorological conditions. Changes in the microclimatic conditions, for example between a shady city park or an open space, can have a stressful effect on the organism such as summer heat stress or winter cold stress (Asseng et al., 2021). While cold stimuli can be mitigated by clothing, this is only possible to a limited extent for summer heat stress.

Due to the predicted increase in the frequency, duration and intensity of heat waves due to climate change, studies on the effects of summer heat stress play an important role (Fischer and Schär, 2010; Wouters et al., 2017; Guerreiro et al., 2018). The consequences will also be more severe in cities during day and night than in the surrounding non-built-up areas. Human-biometeorological research has introduced various thermal assessment indices to investigate heat stress, of which the Physiologically Equivalent Temperature (PET) and the Universal Thermal Climate Index (UTCI) are the most widely used. In order to calculate these assessment indices, meteorological quantities such as air temperature, humidity, wind speed and the mean radiation temperature (T_{mrt}) calculated from the short- and long-wave radiation fluxes must be gathered in their spatio-temporal variability, since only the combined effect of these quantities fully represents the heat load. Studies using regional climate projections have been able to show that the human-biometeorological stress periods will further intensify with increasing climate change. In Freiburg (Germany), for example, the number of days with high heat stress doubles from 25 to 54 days by the end of this century compared to the period 1961–1990 (A1B scenario; Fig. 20).

The PET is controlled by the spatial variability of T_{mrt}, i.e. by differences in the proportions of short- and long-wave radiant flux densities integrated from all six spatial directions. Thus, PET is strongly influenced by urban geometry or shading by buildings or street trees and differs significantly from the characteristics of urban air temperature. By taking wind speed and humidity into account, PET represents a thermal evaluation index that uses the conditions indoor under which a person would feel thermally comfortable as reference conditions for calculating the thermal evaluation, i.e. physiological equivalent (VDI 3787 Part 2).

For the urban area of Berlin, the relationship between the microclimate of an LCZ (cf. Section 2.1) and the PET was studied (Langer et al., 2021). The highest PET values were measured in the LCZ 'open-high rise', which has the highest radiant flux densities during daytime hours due to the highest ψ_{sky} of all urban LCZs (= 0.44). In particular, open squares or wide street canyons with a large ψ_{sky} are usually characterized by low thermal comfort and high summer heat load. The literature depicts a clear relationship between PET as well as the exposure of a street canyon (street orientation), the height-to-width ratio of the adjacent development (aspect ratio), and ψ_{sky} or building height (Ali-Toudert and Mayer, 2007; Yahia et al., 2018). Climate-sensitive planning and design (e.g. optimized height-to-width ratio of street canyons, shading by street trees or solar sails) can achieve significant reductions in heat stress situations during daytime hours (Errel et al., 2011; Nouri et al., 2017). This is especially true for dry and hot cli-

mates with high solar elevations and corresponding solar radiation flux densities.

9 Cities and global climate change

Cities will particularly be influenced by the impacts of global climate change, as an increase in temperature, heat stress, and extreme events (drought, heavy rainfall) will affect areas with high population densities. The occurrence of heat waves is of particular importance for cities, as they can result in a significant intensification of the UHI-effect (Li and Bou-Zeid, 2013). In a model study for Belgium, it was shown that the projected increase in urban heat stress by the middle of the 21st century will be about twice as high as in their surrounding areas (Wouters et al., 2017). Guerreiro et al. (2018) applied climate projections from global climate models to 571 European cities indicating that the number of days with heat waves will clearly increase, with a range of from 4 % for Trondheim to 69 % for Lefkosia in Cyprus. In addition, the maximum air temperature will intensify during heat waves, by about 1.5 K in Helsinki and up to 14 K in Innsbruck. The evidence of further expansion of urban sealed areas and amplification of urban climate effects is highlighted in the recent IPCC report. It is stated that 'there is (1) very high confidence (robust evidence and high agreement) that future urbanization will amplify the projected air temperature warming irrespective of the background climate and there is (2) evidence for the combination of future urban development and more frequent occurrence of extreme climatic events, such as heat waves' (IPCC, 2021).

The health effects caused by thermal stress are evident in increased morbidity and mortality rates, especially during heat episodes, compared to the surrounding area. The thermal stress of urban areas is due to not only the high air and surface temperatures prevailing during the day, but also to the reduced cooling of the urban fabric at night. The UHI values that occur during heat waves can be significantly higher than "normal" summer values (Unger et al., 2020). Much less research has been carried out on the effects of extreme cold periods on the well-being of the urban population. A Spanish study for the region of Madrid found a higher number of cold spells in comparison to heat waves, and a higher urban vulnerability to cold than in the neighbouring countryside. The main risk factor was due to the different demographic structure of the city, i.e. an increased number of urban residents >64 years (Lopez-Bueno et al., 2021).

If thermal stress is simultaneously occurring with increased concentrations of gaseous and particulate pollutants, the mortality may increase (e.g., Breitner et al., 2014; Burkart et al., 2013; Hennig et al., 2018). During dry and warm conditions with strong global radiation secondary pollutants such as ozone and particulate matter can be produced if appropriate precursor gases prevail, e.g. secondary organic aerosol (SOA) from biogenic hydrocarbons (BVOC, e.g. isoprene; Grote, 2019; Wagner and Kuttler, 2014; Mozaffar et al., 2020) through gas-to-particle conversion.

Since the production of certain plant pollens is enhanced by both elevated CO_2 and air pollution concentrations and high air temperatures (Kaminski and Glod, 2011), increased allergy-causing proteins are released from pollen – despite generally lower urban vegetation density. High air temperatures and CO_2 concentrations in mugwort pollen (genus Ambrosia, C3-limited plant), for example, stimulate the production of the allergenic protein Amb a1 and thus cause immune reactions (Ziska and Caulfield, 2000; Ziska et al., 2003). A comparable situation applies to a protein from birch pollen (Bet v1), which is also allergenic and is titrated by high NO_x concentrations (Pöschl, 2005). Long-term studies (1990–2018) underline that due to the global temperature increase, the pollen season in North America was extended by 20 days and pollen concentrations increased by 21 % (Anderegg et al., 2021).

Cities can also be vulnerable to the effects of climate change from a hydrological perspective, as heavy rainfall can lead to flooding and damage to buildings and infrastructure. In addition, a high number of cities in coastal areas are affected by sea-level rise. According to the UN, half of the global urban population lives in a coastal strip of about 100 km, and a total of three-quarters of the large cities are located in this narrow coastal area.

Cities, despite their small share of less than 1 % of the terrestrial land surface (Schneider et al., 2009), are significant global sources of anthropogenic GHG and thus not only affected but also drivers of climate change. Cities account for around 78 % of global energy consumption and emit more than 70 % of global anthropogenic CO_2 (Cleugh and Grimmond, 2012; Moran et al., 2018). At the same time, the 100 cities with the largest carbon footprint are responsible for 18 % of the total global carbon footprint (Moran et al., 2018). The main sources of urban CO_2-emissions are combustion processes in industry, households and transport. Hence, cities offer significant potential to contribute to GHG emission reductions through a sustainable, efficient and largely carbon neutral way of living and doing business.

However, which measures can be recommended by urban climatology to adapt to climate change, especially to urban warming and flooding? In addition to the global reduction of GHG (mitigation), four adaptation measures are relevant on the local scale: shading (incl. albedo enhancement), greening, ventilation and rainwater management.

Shading, which may be provided artificially (e.g., structural shading elements) or naturally by vegetation (e.g., trees or tall shrubs), primarily ensures a reduction in surface and radiation temperature and thus a strong reduction in long-wave radiation compared to the sun-exposed area. Compared to artificial shading, those of a natural surrounding are more effective, since in addition to the reduced release of radiant heat through the shadow

effect, energy is also partitioned into Q_E through transpiration. Shade under large-crowned trees should also provide optimal UV protection for people spending time there.

In addition to shading, light-coloured building surfaces (roofs and facades) may lower their surface temperature by albedo enhancement. This, however, creates an additional – rather negative – glare effect on people standing in front of the buildings in the case of bright facades (Lee and Mayer, 2018). Moreover, the application of thermochromic paints, the colour of which depends on the prevailing thermal conditions (light in case of strong irradiation and dark in case of low irradiation), might be a solution for house paints to prevent overheating in summer and cooling in winter.

Greening is predominantly composed of lawns, shrubs and tree stands, as well as facade and roof greening (Pfoser et al., 2013, Pauleit et al., 2019). During prolonged high summer temperatures, sufficient watering of the plants should be ensured. Lawns in particular can completely lose their cooling effect if they are exposed to long periods of severe drought. In addition, photosynthetic capacity and thus the potential for CO_2 uptake may be reduced as a result of drought (Konopka et al., 2021). The advantage of tree- and shrub-covered stands compared to lawns is the higher transpiration and interception, whereby greater cooling effects are achieved via a higher Q_E. Green facades and roofs primarily lead to an improvement in the climatic conditions on the building scale. However, if there is a large number of such green areas, summation effects could lead to climatic improvements at street or even district level.

Ventilation of an urban area plays an important role, especially during heat waves. The supply of cooler rural air in the night depends on its volume flow and penetration depth into the urban fabric (Gross, 2019). Ventilation paths connecting the surrounding area with the city centre should therefore have sufficient width and be designed with as few obstacles as possible (Grunwald et al., 2020).

Cities should have a decentralized **rainwater management** system. Structural measures for example can serve to protect against flooding and inundation: By installing underground water storage to provide for irrigation during periods of drought ("sponge city principle") and by providing infiltration areas in the form of deep beds and tree trenches. Various VDI guidelines (e.g. VDI 3787 part 8) provide further information on how to solve the above-mentioned problems, especially on the topic of urban development and global climate change. A recent overview of on how urban planning and architecture might benefit from findings of urban climate research is documented in Fallmann and Emeis (2020).

Acknowledgements

The authors would like to thank the following persons: Tobias Bitz (Technische Universität Braunschweig) and Lubov Kronhardt who helped with the manuscript layout and literature compilation. We thank Jannik Heusinger (Technische Universität Braunschweig) for proof-reading and commenting the final manuscript, Peter Hupfer (Berlin) for critical comments on an earlier version of the manuscript, and the two anonymous reviewers for their constructive critics which led to an improvement of the manuscript.

References

Ali-Toudert, F., Mayer, H., 2007: Thermal comfort in an east–west oriented street canyon in Freiburg (Germany) under hot summer conditions. Theoretical and Applied Climatology, 87(1): 223–237.

Allwine, K.J., M.J. Leach, L.W. Stockham, J.S. Shinn, R.P. Hosker, J.F. Bowers, J.C. Pace, 2004: Overview of Joint Urban 2003. – An atmospheric dispersion study in Oklahoma City. – Seattle, WA. USA.

Anderegg, W.L.R., J.T. Abatzoglou, L.D.L. Anderegg et al., 2021: Anthropogenic climate change is worsening North American pollen seasons. – PNAS **118**, e2013284118. DOI: 10.1073/pnas.2013284118.

Antoszewski, P., D. Świerk, M. Krzyżaniak, 2020: Statistical Review of Quality Parameters of Blue-Green Infrastructure Elements Important in Mitigating the Effect of the Urban Heat Island in the Temperate Climate (C) Zone. – Int. J. Env. Res. Public Health **17**, DOI:10.3390/ijerph17197093.

Asseng, S., D. Spänkuch, I.M. Hernandez-Ochoa, J. Laporta, 2021: The upper temperature thresholds of life. – Lancet Planet. Health **5**, e378–e385, DOI:10.1016/S2542-5196(21)00079-6.

Auer, I., R. Böhm, H. Mohnl, 1989: Klima von Wien. Eine anwendungsorientierte Klimatographie. – Zentralanstalt für Meteorologie, Wien, 270 pp.

Baklanov, A., C. Grimmond, D. Carlson, D. Terblanche, X. Tang, V. Bouchet, B. Lee, Langendijk, R.K. Kolli, A. Hovsepyan, 2018: From urban meteorology, climate and environment research to integrated city services. – Urban Climate **23**, 330–341, DOI:10.1016/j.uclim.2017.05.004.

Balchin, W.G.V., N. Pye, 1947: A micro-climatological investigation of Bath and the surrounding district. – Quart. J. Roy. Meteor. Soc. **73**, 297–323, DOI:10.1002/qj.49707331706.

Behre, O., 1908: Das Klima von Berlin. Eine meteorologisch-hygienische Untersuchung. – Otto Sale, Berlin, 158 pp.

Blankenstein, S., W. Kuttler, 2004: Impact of street geometry on downward longwave radiation and air temperature in an urban environment. – Meteorol. Z. **13**, 373–379, DOI: 10.1127/0941-2948/2004/0013-0373.

Bornstein, R.D., 1975: The Two-Dimensional URB-MET Urban Boundary Layer Model. – J. Appl. Meteor. **14**, 1459–1477, DOI:10.1175/1520-0450(1975)014<1459:TTDUUB>2.0.CO;2.

Breitner, S., K. Wolf, R.B. Devlin, et al., 2014: Short-term Effects of Air Temperature on Mortality and Effect Modification by Air Pollution in three Cities of Bavaria, Germany: a Time-Series Analysis. – Sci. Total Env. **485**, 49–61.

Brooks, C., 1952: Selective annotated bibliography on urban climate. – Meteor. Abstr. Bibliography **3**, 734–773.

Bruse, M., 1999: Die Auswirkungen kleinskaliger Umweltgestaltung auf das Mikroklima. – Univ. Bochum. DOI: 10.23689/fidgeo-440.

Burkart, K., P. Canario, S. Breitner, 2013: Interactive short-term Effects of Equivalent Temperature and Air Pollution on human Mortality in Berlin and Lisbon. – Env. Poll. **183**, 54–63.

Cermak, J.E., A.G. Davenport, E.J. Plate, D.X. Viegas, 1995: Wind Climate in Cities. – Kluwer Academic Publ., 772 p.

Chandler, T., 1970: Selected bibliography on urban climate. – WMO Publ. No. 276, TP 155, Geneva.

Changnon, S.A. (Ed.), 1981: Metromex. A review and summary. – Amer. Meteor. Soc., Boston, Mass., 181 pp.

Chapman, L., C. Bell, S. Bell, 2016: Can the crowdsourcing data paradigm take atmospheric science to a new level? A case study of the urban heat island of London quantified using Netatmo weather stations. – Int. J. Climatol. **37**, 3597–3605, DOI:10.1002/joc.4940.

Christen, A., R. Vogt, 2004: Energy and radiation balance of a central European city. – Int. J. Climatol. **24**, 1395–1421, DOI: 10.1002/joc.1074.

Christen, A. 2019: Vertikale Gliederung der Stadtatmosphäre. Kap. 1.3. – In: Lozán, J.L., S.-W. Breckle, H. Grassl, W. Kuttler, A. Matzarakis (Hrsg.). Warnsignal Klima: Die Städte. – Published online, www.klima-warnsignale.uni-hamburg.de, DOI:10.2312/warnsignal-klima.die-staedte.05.

Cleugh, H., S. Grimmond, 2012: Chapter 3 – Urban Climates and Global Climate Change. – In: Henderson-Sellers, A., K. Mcguffie, K. Macguffie (Eds.): The Future of the World's Climate (Second Edition). – Elsevier, Boston, 47–76, DOI:10.1016/B978-0-1386917-3.00003-8.

Conradie, E.H., P.G. Van Zyl, J.J. Pienaar, J.P. Beukes, C. Galy-Lacaux, A.D. Venter, G.V. Mkhatshwa, 2016: The chemical composition and fluxes of atmospheric wet deposition at four sites in South Africa. – Atmos. Env. **146**, 113–131, DOI:10.1016/j.atmosenv.2016.07.033.

Crawford, B., A. Christen, 2015: Spatial source attribution of measured urban eddy covariance CO2 fluxes. – Theor. Appl. Climatol. **119**, 733–755, DOI:10.1007/s00704-014-1124-0.

Demuzere, M., J. Kittner, B. Bechtel, 2021: LCZ Generator: A Web Application to Create Local Climate Zone Maps. – Front. Env. Sci. **9**. DOI:10.3389/fenvs.2021.637455.

Droste, A.M., B.G. Heusinkveld, B., D. Fenner, G.-J. Steeneveld, 2020: Assessing the potential and application of crowdsourced urban wind data. – Quart. J. Roy. Meteor. Soc. **146**, 2671–2688, DOI:10.1002/qj.3811.

Erell, E., D. Pearlmutter, T. Williamson, 2011: Urban microclimate: designing the spaces between buildings. – Earthscan, London, Washington, 266 pp.

Evelyn, J., 1661: Fumifugium: Or the inconvenience of the air and smoke of London dissipated. – National Smoke Abatement Society, Manchester 1933, Oxford, England, 43 pp.

Fallmann, J., S. Emeis, 2020: How to bring urban and global climate studies together with urban planning and architecture? –Develop. Built. Env. **4**, 100023.

Fallmann, J., M. Barra, V. Kumar, H. Tost, 2021: Impact of urban imperviousness on boundary layer meteorology and air chemistry on a regional scale. – Meteorol. Z. **30**, 349–367, DOI:10.1127/metz/2021/1075.

Fensterbusch, C., 1991: De architectura libri decem (Autor: Vitruvius). – Wissenschaftliche Buchgesellschaft, Darmstadt, 585 pp.

Fischer, E.M., C. Schär, 2010: Consistent geographical patterns of changes in high-impact European heatwaves. – Nature Geosci. **3**, 398–403, DOI:10.1038/ngeo866.

Flanner, M.G., 2009: Integrating anthropogenic heat flux with global climate models. – Geophys. Res. Lett. **36**, L02801, DOI:10.1029/2008GL036465.

Foken, T. (Ed.), 2021: Springer handbook of atmospheric measurements. – Springer, Cham, 1748 pp.

Ginzburg, A.S., S.A. Dokukin, 2019: Anthropogenic heat fluxes in urban agglomerations and their impact on meteorological processes. – IOP Conf. Ser.: Earth Environ. Sci. **386**, 12049, DOI:10.1088/1755-1315/386/1/012049.

Goldbach, A., W. Kuttler, 2012: Quantification of turbulent heat fluxes for adaptation strategies within urban planning. – Int. J. Climatol. DOI:10.1002/joc.3437

Grange, S.K., H. Lötscher, A. Fischer, et al., 2020: Evaluation of equivalent black carbon source apportionment using observations from Switzerland between 2008 and 2018. – Atmos. Meas. Tech. **13**, 1867–1885, https://www.atmos-meas-tech.net/13/1867/2020/.

Grimmond, C.S., G. Carmichael, H. Lean, A. Baklanov, et al., 2015: Urban-Scale environmental prediction systems. – In: Brunet, G., S. Jones, P. Ruti (Eds): Seamless Prediction of the Earth-System: from minutes to months. World Meteorological Organization, Geneva, 347–370. ISBN 9789263111562.

Groh, J., V. Slawitsch, M. Herndl, A. Graf, H. Vereecken, T. Pütz, 2018: Determining dew and hoar frost formation for a low mountain range and alpine grassland site by weighable lysimeter. – J. Hydrol. **563**, 372–381, DOI:10.1016/j.jhydrol.2018.06.009.

Gross, G., 2019: On the self-ventilation of an urban heat island. – Meteorol. Z. **28**, 87–92.

Gross, G., C. Etling, 2003: Numerische Simulationsmodelle. – promet **30**, 28–38.

Grote, R., S.M. Ghirardo, J.P. Schnitzler, 2019: A New Modeling Approach for Estimating Abiotic and Biotic Stress-Induced de novo Emissions of Biogenic Volatile Organic Compounds from Plants. – Front. For. Glob. Change **2**, 6, DOI: 10.3389/ffgc.2019.00026.

Grunwald, L., M. Kossmann, S. Weber, 2019: Mapping urban cold-air paths in a Central European city using numerical modelling and geospatial analysis. – Urban Climate **29**, 100503, DOI:10.1016/j.uclim.2019.100503.

Grunwald, L., A.-K. Schneider, B. Schröder, S. Weber, 2020: Predicting urban cold-air paths using boosted regression trees. – Lands. Urban Plan. **201**, 103843, DOI:10.1016/j.landurbplan.2020.103843.

Guerreiro, S.B., R.J. Dawson, C. Kilsby, E. Lewis, A. Ford, 2018: Future heat-waves, droughts and floods in 571 European cities. – Env. Res. Lett. **13**, 34009, DOI:10.1088/1748-9326/aaaad3.

Hamdi, R., H. Kusaka, Q.-V. Doan, P. Cai, H. He, G. Luo, W. Kuang, S. Caluwaerts, F. Duchêne, B. van Schaeybroek, P. Termonia, 2020: The State-of-the-Art of Urban Climate Change Modeling and Observations. – Earth Sys. Env. **4**, 631–646.

Hann, J., 1885: Über den Temperaturunterschied zwischen Stadt und Land. – Z. Österr. Ges. Meteor. **20**, 457–465.

Harlass, R., 2008: Verdunstung in bebauten Gebieten. – Dissertation, Techn. Univ. Dresden.

Helbig, A., 1987: Beiträge zur Meteorologie der Stadtatmosphäre. – Abh. Met. Dienst DDR, Nr. **137**, Akademie-Verlag Berlin.

Helbig, A., J. Baumüller, M.J. Kerschgens, 1999: Stadtklima und Luftreinhaltung. – Springer Berlin Heidelberg, Berlin, Heidelberg, 467 pp.

Hennig, F., H. Quass, B. Hellack et al., 2018: Ultrafine and Fine Particle Number and Surface Area Concentrations and Daily Cause-Specific Mortality in the Ruhr-Area, Germany, 2009–2014. – Env. Health Persp. **126**. DOI:10.1289/EHP2054.

Henninger, S., S. Weber, 2020: Stadtklima. – Ferdinand Schöningh, Paderborn, 260 pp.

Heusinger, J., S. Weber, 2017: Surface energy balance of an extensive green roof as quantified by full year eddy-covariance measurements. – Sci. Total Env. **577**, 220–230.

Hidalgo, J., G. Pigeon, V. Masson, 2008: Urban-breeze circulation during the CAPITOUL experiment: observational data

analysis approach. – Meteor. Atmos. Phys. **102**, 223–241, DOI:10.1007/s00703-008-0329-0.

Hong, J.W., J. Hong, J. Chun, et al., 2019: Comparative assessment of net CO2 exchange across an urbanization gradient in Korea based on eddy covariance measurements. – Carbon Balance Manage. **14**, 13. DOI:10.1186/s13021-019-0128-6.

Holst, J., H. Mayer, 2011: Impacts of street design parameters on human-biometeorological variables. – Meteorol. Z. **20**, 541–552, DOI:10.1127/0941-2948/2011/0254.

Howard, L., 1818: The Climate of London. Deduced from Meteorological Observations: Volume 1. – Cambridge University Press, Cambridge, 376 pp.

Hughes, R.N., P. Brimblecombe, 1994: Dew and guttation: formation and environmental significance. – Agricult. Forest Meteor. **67**, 173–190.

Hupfer, P., F.M. Chmielewski, 1990: Das Klima von Berlin. – Akademie Verlag, Berlin, 288 pp.

Hupfer, P., W. Kuttler (Eds), 2006: Witterung und Klima. Eine Einführung in die Meteorologie und Klimatologie, 12. A. – Teubner, Stuttgart, 554 pp.

Inoue, T., F. Kumura, 2009: Fair-weather cumulus clouds forming over urban areas around Tokyo. – 7th Int. Conf. Urban Climate, 29 June–3 July 2009, Yokohama, Japan.

IPCC, 2021: Climate Change 2021: The Physical Science Basis. Contribution of Working Group I to the Sixth Assessment Report of the Intergovernmental Panel on Climate Change. Masson-Delmotte, V., P. Zhai, A. Pirani, S.L. Connors, C. Péan, S. Berger, N. Caud, Y. Chen, L. Goldfarb, M.I. Gomis, M. Huang, K. Leitzell, E. Lonnoy, J.B.R. Matthews, T.K. Maycock, T. Waterfield, O. Yelekçi, R. Yu, B. Zhou (Eds.). – Cambridge University Press.

Jasek-Kaminska, A., M. Znoch, P. Wachniew, K. Rozanski, 2020: Urban CO2 Budget: Spatial and Seasonal Variability of CO2 Emissions in Krakow, Poland. – Atmosphere **11**, 629; DOI:10.3390/atmos11060629.

Jauregui, E., 1973: The urban climate of Mexico City. – Erdkunde **27**, DOI:10.3112/1973.04.06.

Jendritzky, G., W. Sönning, H.J. Swantes, 1979: Ein objektives Bewertungsverfahren zur Beschreibung des thermischen Milieus in der Stadt- und Landschaftsplanung ("Klima-Michel-Modell"). – Schroedel, Hannover, 85 pp.

Junkermann, W., J. Hacker, 2022: Unprecedented levels of ultrafine particles, major sources, and the hydrological cycle. Sci. Reports **12**, 7410.

Kassener, C., 1910: Die meteorologischen Grundlagen des Städtebaues. – Ernst & Sohn, Berlin.

Knauss, D., 1901: Die Stuttgarter Stadterweiterung mit volkswirtschaftlichen hygienischen und künstlerischen Gutachten. – Stadtschultheissenamt Stuttgart.

Konopka, J., J. Heusinger, S. Weber, 2021. Extensive Urban Green Roof Shows Consistent Annual Net Uptake of Carbon as Documented by 5 Years of Eddy-Covariance Flux Measurements. – J. Geophys. Res. Biogeosci. **126**, DOI:10.1029/2020JG00587.

Kratzer, A., 1937, 1956: Das Stadtklima. – F. Vieweg & Sohn, Braunschweig, 184 pp.

Küpper, M., U. Quass, A.C. John, et al., 2018: Contributions of carbonaceous particles from fossil emissions and biomass burning to PM10 in the Ruhr area, Germany. – Atmos. Env **189**, 174–186

Kuttler, W., 1979a: London-Smog und Los Angeles-Smog. – Erdkunde **33**, 236–240, DOI:10.3112/1979.03.07.

Kuttler, W., 1979b: Einflußgrößen gesundheitsgefährdender Wetterlagen und deren bioklimatische Auswirkungen auf potenzielle Erholungsgebiete. Dargestellt am Beispiel des Ruhrgebietes und des Sauerlandes. – Zugl.: Bochum, Univ., Diss. 1978. – Schöningh, Paderborn, 101 pp.

Kuttler, W., 2013: Klimatologie. 2. Aufl. – UTB 3099. Schöningh Verlag, Paderborn, 306. S.

Kuttler, W., S. Weber, J. Schonnefeld, A. Hesselschwerdt, 2007: Urban/rural atmospheric water vapour pressure differences and urban moisture excess in Krefeld, Germany. – Int. J. Climatol. **27**, 2005–2015, DOI:10.1002/joc.1558.

Kuttler, W., A. Miethke, D. Dütemeyer, A.-B. Barlag, 2015: Das Klima von Essen. = The climate of Essen. – Westarp Wissenschaft, Hohenwarsleben, 249 pp.

Landsberg, H.E., 1979: Atmospheric changes in a growing community (the Columbia, Maryland experience). – Urban Ecology **4**, 53–81, DOI:10.1016/0304-4009(79)90023-8.

Landsberg, H.E., 1981: The urban climate. – Academic Press, New York, 275 pp.

Langer, I., E. Fakharizadehshirazi, J. Werner, 2021: Spatial variation of physiologically equivalent temperature in different Local Climate Zones of a large city during a hot spell. – Meteorol. Z. **30**, 115–125, DOI:10.1127/metz/2020/0996.

Lee, T.F., 1987: Urban clear islands in California Central Valley fog. – Mon. Wea. Rev. **115**, 1794–1796, DOI:10.1175/1520-0493(1987)115%3C1794:UCIICC%3E2.0.CO;2.

Lee, H., H. Mayer, 2018: Thermal comfort of pedestrians in an urban street canyon is affected by increasing albedo of building walls. – Int. J. Biometeorol. **62**, 1199–1209, DOI:10.1007/s00484-018-1523-5.

Li, D., E. Bou-Zeid, 2013: Synergistic Interactions between Urban Heat Islands and Heat Waves: The Impact in Cities Is Larger than the Sum of Its Parts. – J. Appl. Meteor. Climatol. **52**, 2051–2064, DOI:10.1175/JAMC-D-13-02.1.

Li, X., W. Fan, L. Wang, et al., 2021: Effect of urban expansion on atmospheric humidity in Beijing-Tianjin-Hebei urban agglomeration. – Sci. Total. Env. **759**, 144305, DOI:10.1016/j.scitotenv.2020.144305.

Lindberg, F., C.S.B. Grimmond, N. Yogeswaran, S. Kotthaus, L. Allen, 2013: Impact of city changes and weather on anthropogenic heat flux in Europe 1995–2015. – Urban Climate **4**, 1–15, DOI:10.1088/1748-9326/aa9f73.

Liu, B., Z. Xie, P. Qin, et al., 2021: Increases in Anthropogenic Heat Release from Energy Consumption Lead to More Frequent Extreme Heat Events in Urban Cities – Advan. Atmos. Sci. **38**, 430–445.

Lopez-Bueno, J.A., M.A. Navas-Martin, J. Diaz, I.J. Miron, M.J. Luna, G. Sanchez-Martinez, D. Culqui, C. Linares, 2021: The effect of cold waves on mortality in urban and rural areas of Madrid. – Env. Sci. Eur. **33**, DOI:10.1186/s12302-021-00512-z.

Lotteraner, C., M. Piringer, 2016: Mixing-Height Time Series from Operational Ceilometer Aerosol-Layer Heights. – Bound.-Layer Meteor. **161**, 265–287, DOI:10.1007/s10546-016-0169-2.

Lowry, W.P., 1977: Empirical Estimation of Urban Effects on Climate: A Problem Analysis. – J. Appl. Meteor. **16**, 129–135, DOI:10.1175/1520-0450(1977)016%3C0129:EEOUEO%3E2.0.CO;2.

Ma, L., Y. Wang, Z. Liang, J. Ding, J. SHEN, F. Wei, S. LI, 2021: Changing Effect of Urban Form on the Seasonal and Diurnal Variations of Surface Urban Heat Island Intensities (SUHIIs) in More Than 3000 Cities in China. – Sustainability **13**, 2877, DOI:10.3390/su13052877.

Manoli, G., S. Fatichi, M. Schläpfer, K. Yu, T.W. Crowther, N. Meili, P. Burlando, G.G. Katul, E. Bou-Zeid, 2019: Magnitude of urban heat islands largely explained by climate and population. – Nature **573**, 55–60, DOI:10.1038/s41586-019-1512-9.

Marley, H.G., K.N. Dirks, I. Mckendry, L.F. Weissert, J.A. Salmond, 2021: A Ceilometer-Derived Climatology of

the Convective Boundary Layer Over a Southern Hemisphere Subtropical City. – Bound.-Layer Meteor. **178**, 435–462, DOI: 10.1007/s10546-020-00579-w.

Masson, V., C. Grimmond, T.R. Oke, 2002: Evaluation of the Town Energy Balance (TEB) Scheme with Direct Measurements from Dry Districts in Two Cities. – J. Appl. Meteor. **41**, 1011–1026, DOI:10.1175/1520-0450(2002)041<1011:EOTTEB>2.0.CO;2.

Masson, V., L. Gomes, G. Pigeon, C. Liousse, V. Pont, J.-P. Lagouarde, J. Voogt, J. Salmond, T.R. Oke, J. Hidalgo, D. Legain, O. Garrouste, C. Lac, O. Connan, X. Briottet, S. Lachérade, P. Tulet, 2008: The Canopy and Aerosol Particles Interactions in Toulouse Urban Layer (CAPITOUL) experiment. – Meteor. Atmos. Phys. **102**, 135–157, DOI:10.1007/s00703-008-0289-4.

Masson, V., A. Lemonsu, J. Hidalgo, J. Voogt, 2020a: Urban Climates and Climate Change. – Ann. Rev. Env. Resour. **45**, 411–444.

Masson, V., W. Heldens, F. Bocher, M. Bonhomme, B. Bucher, C. Burmeister, C. de Munck, T. Esch, J. Hidalgo, F. Kanani-Sühring, Y.-T. Kwok, A. Lemonsu, J.-P. Lévy, B. Maronga, D. Pavlik, G. Petit, L. See, R. Schoetter, N. Tornay, A. Votsis, J. Zeidler, 2020b: City-descriptive input data for urban climate models: Model requirements, data sources and challenges. – Urban Climate **31**, 100536.

Matzarakis, A., C. Endler, 2010: Climate change and thermal bioclimate in cities: impacts and options for adaptation in Freiburg, Germany. – Int. J. Biometeorol. **54**, 479–483, DOI: 10.1007/s00484-009-0296-2.

Mayer, H., P. Höppe, 1987: Thermal comfort of man in different urban environments. – Theor. Appl. Climatol. **38**, 43–49, DOI: 10.1007/BF00866252.

Mayer, H., 1988: Results from the research program "STADTKLIMA BAYERN" for urban planning. – Energy Build. **11**, 115–121, DOI:10.1016/0378-7788(88)90027-8.

Mayer, H., W. Beckröge, A. Matzarakis, 1994: Bestimmung von stadtklimarelevanten Luftleitbahnen. – UVP-Report **5**, 265–268.

Meier, F., D. Fenner, T. Grassmann, M. Otto, D. Scherer, 2017: Crowdsourcing air temperature from citizen weather stations for urban climate research. – Urban Climate **19**, 170–191, DOI:10.1016/j.uclim.2017.01.006.

Monteith, J.L., 1957: Dew. – Quart. J. Roy. Meteor. Soc. **83**, 322–341, DOI:10.1002/qj.49708335706.

Moran, D., K. Kanemoto, M. Jiborn, R. Wood, J. Többen, K.C. Seto, 2018: Carbon footprints of 13000 cities. – Environ. Res. Lett. **13**, 64041, DOI:10.1088/1748-9326/aac72a.

Moriyama, M., M. Matsumoto, 1988: Control of urban night temperature in semitropical regions during summer. – Energy Build. **11**, 213–219, DOI:10.1016/0378-7788(88)90037-0.

Mozaffar, A., Y.L. Zhang, M. Fan, et al., 2020: Characteristics of summertime ambient VOCs and their contributions to O3 and SOA formation in a suburban area of Nanjing, China. – Atmos. Res. **240**, DOI:10.1016/J.ATMOSRES.2020.104923.

Mulawa, P.A., S.H. Cadle, F. Lipari, C. C Ang, R. Vandervennet, 1986: Urban dew: Its composition and influence on dry deposition rates. – Atmos. Env. **20**, 1389–1396, DOI: 10.1016/0004-6981(86)90009-0.

Naughton, J., W. McDonald, 2019: Evaluating the Variability of Urban Land Surface Temperatures Using Drone Observations. – Remote Sens. **11**, 1722, DOI:10.3390/rs11141722.

Neumann, J., 1979: Air pollution in Ancient Rome. – Bull. Amer. Meteor. Soc. **60**, 1097.

Niyogi, D., P. Pyle, M. Lei, S.P. Arya, C.M. Kishtawal, M. Shepherd, F. Chen, B. Wolfe, 2011: Urban Modification of Thunderstorms: An Observational Storm Climatology and Model Case Study for the Indianapolis Urban Region. – J. Appl. Meteor. Climatol. **50**, 1129–1144, DOI: 10.1175/2010JAMC1836.1.

Nouri, A.S., J.P. Costa, A. Matzarakis, 2017: Examining default urban-aspect-ratios and sky-view-factors to identify priorities for thermal-sensitive public space design in hot-summer Mediterranean climates: The Lisbon case. – Build. Env. **126**, 442–456.

Oke, T.R., 1974: Review of urban climatology 1968–1973. – WMO Tech. Note **134**, 132 pp.

Oke, T.R., 1979: Review of urban climatology 1973–1976. – WMO Tech. Note **169**, 100 pp.

Oke, T.R., G. Mills, A. Christen, J.A. Voogt, 2017: Urban Climates. – Cambridge University Press, Cambridge, 525 pp.

Pagenkopf, A., 2009: Verification of urban-induced precipitation for a central European major city. 7th Int. Conf. Urban Climate 29 June – 3 July 2009, Yokohama, Japan.

Pauleit, S., E. Andersson, B. Anton, et al., 2019: Urban green infrastructure – connecting people and nature for sustainable cities. – Urban Forest. Urban Greening **40**, 1–3.

Peppler, A., 1929: Das Auto als Hilfsmittel der Meteorologischen Forschung. – Z. angew. Meteorol. **46**, 305–308.

Pfoser, N., N. Jenner, J. Henrich, et al., 2013: Gebäude, Begrünung, Energie. Potenziale und Auswirkungen. – Forschungsbericht TU Darmstadt.

Pichler, P.-P., T. Zwickel, A. Chavez, T. Kretschmer, J. Seddon, H. Weisz, 2017: Reducing Urban Greenhouse Gas Footprints. – Sci. Rep. **7**, 14659, DOI:10.1038/s41598-017-15303-x.

Pöschl, U., 2005: Atmosphärische Aerosole: Zusammensetzung, Transformation, Klima- und Gesundheitseffekte. – Angew. Chemie, 117, 7690–7712.

Raasch, S., M. Schröter, 2001: PALM – A large-eddy simulation model performing on massively parallel computers. – Meteorol. Z. **10**, 363–372, DOI:10.1127/0941-2948/2001/0010-0363.

Reitebuch, D., A. Strassburger, S. Emeis, W. Kuttler, 1998: SODAR-Analyse von Turbulenz und Wind während sekundärer nächtlicher Ozonmaxima in einem urbanen Park. – Ann. Meteorol. **37**, 187–188.

Ren, C., E.Y. Ng, L. Katzschner, 2011: Urban climatic map studies: a review. – Int. J. Climatol. **31**, 2213–2233, DOI: 10.1002/joc.2237.

Richards, K., 2005: Urban and rural dewfall, surface moisture, and associated canopy-level air temperature and humidity measurements for vancouver, canada. – Bound.-Layer Meteor. **114**, 143–163, DOI:10.1007/s10546-004-8947-7.

Richards, K., T.R. Oke, 2002: Validation and results of a scale model of dew deposition in urban environments. – Int. J. Climatol. **22**, 1915–1933.

Rosenfeld, D., 2000: Suppression of rain and snow by urban and industrial air pollution. – Science **287**, 1793–1796, DOI: 10.1126/science.287.5459.1793.

Rotach, M.W., R. Vogt, C. Bernhofer, E. Batchvarova, A. Christen, A. Clappier, B. Feddersen, S.-E. Gryning, G. Martucci, H. Mayer, V. Mitev, T.R. Oke, E. Parlow, H. Richner, M. Roth, Y.-A. Roulet, D. Ruffieux, J.A. Salmond, M. Schatzmann, J.A. Voogt, 2005: BUBBLE – an Urban Boundary Layer Meteorology Project. – Theor. Appl. Climatol. **81**, 231–261, DOI:10.1007/s00704-004-0117-9.

Sachweh, M., P. Köpke, 1995: Radiation fog and urban climate. – Geophys. Res. Lett. **22**, 1073–1076.

Sailor, D.J., M. Georgescu, J.M. Milne, M.A. Hart, 2015: Development of a national anthropogenic heating database with an extrapolation for international cities. – Atmos. Env. **118**, 7–18, DOI:10.1016/j.atmosenv.2015.07.016.

Scherer, D., F. Ament, S. Emeis, U. Fehrenbach, B. Leitl, K. Scherber, C. Schneider, U. Vogt, 2019: Three-Dimensional Observation of Atmospheric Processes in Cities. – Meteorol. Z. **28**, 121–138, DOI:10.1127/metz/2019/0911.

Schirmer, H., W. Kuttler, J. Löbel, K. Weber, 1993: Lufthygiene und Klima. Ein Handbuch zur Stadt- und Regionalplanung. – Springer, Berlin, Heidelberg, 526 pp.

Schlünzen, K.H., S. Grimmond, A. Baklanov (Eds), 2022: Guidance on Measuring, Modelling and Monitoring the Canopy Layer Urban Heat Island (CL-UHI). – World Meteorological Organization (WMO), Report WMO-No. **1292.**

Schmidt, W., 1930: Kleinklimatische Aufnahmen durch Temperaturmessfahrten. – Meteorol. Z. **47**, 92–106.

Schneider, A., M.A. Friedl, D. Potere, 2009: A new map of global urban extent from MODIS satellite data. – Env. Res. Lett. **4**, 44003, DOI:10.1088/1748-9326/4/4/044003.

Schütz, M., 1996: Anthropogene Niederschlagsmodifikationen im komplexurbanen Raum am Beispiel des Ruhrgebiets. – Dissertation, Fachbereich 9, Universität Essen, Essen, 151 pp.

Seckmeyer, G., M. Schrempf, 2018: How much shade outdoors is healthy? – NIWA UV Workshop, Wellington, 4–6 Apr, 2018, www.niwa.co.nz/atmosphere/uv-ozone/uv-science-workshops/2018-uv-workshop.

Seino, N., R. Oda, H. Sugawara, T. Aoyagi, 2018: Observations and Simulations of the Mesoscale Environment in TOMACS Urban Heavy Rain Events. – J. Meteor. Soc. Japan **96A**, 221–245, DOI:10.2151/jmsj.2018-029.

Sham, S., 1979: Aspects of Air Pollution Climatology in a Tropical City: A Case of Kuala Lumpur–Petaling Jaya, Malaysia. – Universiti Kebangsaan Malaysia Press, 344 pp.

Sham, S., 1990: Urban climatology in Malaysia: An overview. – Energy Build. **15**, 105–117, DOI:10.1016/0378-7788(90)90121-X.

Sharma, A., D.J. Wuebbles, R. Kotamarthi, 2021: The Need for Urban-Resolving Climate Modeling Across Scales. – AGU Advances **2**, e2020AV000271.

Shepherd, J.M., 2005: A review of current investigations of urban-induced rainfall and recommendations for the future. – Earth Interact. **9**, 1–27, DOI:10.1175/EI156.1.

Sicard, P., E. Agathokleous, A. De Marco, E. Paoletti, V. Calatayud, 2021: Urban population exposure to air pollution in Europe over the last decades. – Env. Sci. Eur. **33**, 28, DOI:10.1186/s12302-020-00450-2.

Simmonds, I., K. Keay, 1997: Weekly cycle of meteorological variations in Melbourne and the role of pollution and anthropogenic heat release. – Atmos. Env. **31**, 1589–1603, DOI:10.1016/S1352-2310(96)00344-5.

Simon, H., F. Fallmann, T. Kropp, H. Tost, M. Bruse, 2019: Urban Trees and Their Impact on Local Ozone Concentration – A Microclimate Modeling Study. – Atmosphere **10**, 154, DOI:10.3390/atmos10030154.

Smith, P., P. Sarricolea, O. Peralta, J.P. Aguila, F. Thomas, 2021: Study of the urban microclimate using thermal UAV. The case of the mid-sized cities of Arica (arid) and Curicó (Mediterranean), Chile. – Build. Env. **206**, 108372, DOI:10.1016/j.buildenv.2021.108372.

Smith, R.A., 1872: Air and Rain: The Beginnings of a Chemical Climatology. – Longmans, Green and Company, London, 600 pp.

Solcerova, A., 2018: Water as a coolant of cities. – PhD-Thesis, Univ. of Delft, NL.

Steinhauser, F., O. Eckel, F. Sauberer, 1955, 1957, 1959: Klima und Bioklima von Wien. – Teil 1 (123 pp), Teil 2 (136 pp), Teil 3 (136 pp). Österr. Gesell. f. Meteorologie, Wien XIX, Hohe Warte.

Stewart, I.D., T.R. Oke, 2012: Local Climate Zones for Urban Temperature Studies. – Bull. Amer. Meteor. Soc. **93**, 1879–1900, DOI:10.1175/BAMS-D-11-00019.1.

Suarez-Bertoa, R., C. Astorga, 2018: Impact of cold temperature on Euro 6 passenger car emissions. – Env. Poll. **234**, 318–329

Sun, J., W. Birmili, M. Hermann, et al., 2019: Variability of black carbon mass concentrations, sub-micrometer particle. Atmos. Env. **220**, 256–268, DOI:10.1016/j.atmosenv.2018.12.029.

Takano, T., M. Ueyama, 2021: Spatial variations in daytime methane and carbon dioxide emissions in two urban landscapes, Sakai, Japan. – Urban Climate **36**, 100798, DOI:10.1016/j.uclim.2021.100798.

Theeuwes, N.E., J.F. Barlow, A.J. Teuling, C.S.B. Grimmond, S. Kotthaus, 2019: Persistent cloud cover over megacities linked to surface heat release. – NPJ Climate Atmos. Sci. **2**, 15.

Theeuwes, N.E., I.A. Boutle, P.A. Clark, S. Grimmond, 2022: Understanding London's summertime cloud cover. – Quart. J. Roy. Meteor. Soc. **148**, 454–465, DOI:10.1002/qj.4214.

Unger, J., N. Skarbit, A. Kovacs, T. Gal, 2020: Comparison of regional and urban outdoor thermal stress conditions in heatwave and normal summer periods: A case study. – Urban Climate **32**, 100619, DOI:10.1016/j.uclim.2020.100619

Vautard, R., P. Yiou, G.J. van Oldenborgh, 2009: Decline of fog, mist and haze in Europe over the past 30 years. – Nature Geosci. **2**, 115–119, DOI:10.1038/NGEO414.

VDI 3785 Part 1, 2008: Methods and presentation of investigations relevant for planning urban climate. – Beuth Verlag, Berlin.

VDI 3785, Part 2, 2011: Methods of urban and side-related ground-based climate measurements with mobile measurements. – Beuth Verlag, Berlin.

VDI 3787, Part 9, 2004: Provision for climate and air quality in regional planning. – Beuth Verlag, Berlin.

VDI 3787, Part 2, 2008: Methods for the human-meteorological evaluation of climate and air quality for urban and regional planning. Part 1: Climate. – Beuth Verlag, Berlin.

VDI 3787, Part 4, 2020: Methods for describing and evaluating strong and weak winds in build-up areas. – Beuth Verlag, Berlin

VDI 3787, Part 8, 2020: Urban development in view of climate change. – Beuth Verlag, Berlin

VDI 3789, 2019: Interactions between atmosphere and surfaces. Calculation of spectral short-wave and long-wave radiation. – Beuth Verlag, Berlin.

Vivoni, E.R., M. Kindler, Z. Wang, E.R. Pérez-Ruiz, 2020: Abiotic mechanisms drive enhanced evaporative losses under urban oasis conditions. – Geophys. Res. Lett. **47**, DOI:10.1029/2020GL090123.

von Bismarck-Osten, C., W. Birmili, M. Ketzel, A. Massling, T. Petäjä, S. Weber, 2013: Characterization of parameters influencing the spatio-temporal variability of urban aerosol particle number size distributions in four European cities. – Atmos. Env. **77**, 415–429, DOI:10.1016/j.atmosenv.2013.05.029.

Van Pinxteren, D., S. Düsing, A. Wiedensohler, H. Herrmann, 2020: Machine learning 'De-Weathering' of urban NOx data to quantify meteorological impacts at two traffic sites in Germany, Faraday Discussion – Air quality in Megacities. – Online Event, 17–20 November 2020, https://airquality-fd2020-rsc.ipostersessions.com/default.aspx?s=CF-63-8D-59-B1-BB-D8-02-53-79-6E-F1-ED-2F-33-B0.

Vujović, D., N. Todorović, 2018: Urban-rural fog differences in Belgrade area, Serbia. – Theor. Appl. Climatol. **131**, 889–898, DOI:10.1007/s00704-016-2019-z.

Vulova, S., F. Meier, A.D. Rocha, J. Quanz, H. Nouri, B. Kleinschmit, 2021: Modelling urban evapotranspiration using remote sensing, flux footprints, and artificial intelligence. – Sci. Total Environ. **786**, 147293, DOI:10.1016/j.scitotenv.2021.147293.

Wagner, P., W. Kuttler, 2014: Biogenic and anthropogenic isoprene in the near-surface urban atmosphere – a case study in Essen, Germany. – Sci. Total Env. **475**, 104–115, DOI: 10.1016/j.scitotenv.2013.12.026.

Wang, Z., J. Song, P.W. Chan, Y. Li, 2020: The urban moisture island phenomenon and its mechanisms in a high-rise high-density city. – Int. J. Climatol. **41**, E150-E170, DOI:10.1002/joc.6672.

Ward, H.C., S. Kotthaus, C.S.B. Grimmond, A. Bjorkegren, M. Wilkinson, W.T.J. Morrison, J.G. Evans, J.I.L. Morison, M. Iamarino, 2015: Effects of urban density on carbon dioxide exchanges: Observations of dense urban, suburban and woodland areas of southern England. – Env. Poll. **198**, 186–200, DOI:10.1016/j.envpol.2014.12.031.

Weber, S., K. Kordowski, 2010: Comparison of atmospheric turbulence characteristics and turbulent fluxes from two urban sites in Essen, Germany. – Theor. Appl. Climatol. **102**, 61–74, DOI:10.1007/s00704-009-0240-8.

Weickmann, L., H. Ungeheuer, H. de Rudder et al., 1952: Klima, Wetter, Mensch. 2. A., Quelle und Meyer, 293 S.

Wessolek, G., 2001: Bodenüberformung und -versiegelung. – In: Handbuch der Bodenkunde, 1–35, DOI:10.1002/9783527678495.hbbk2001002.

Wessolek, G., M. Facklam, 1997: Standorteigenschaften und Wasserhaushalt von versiegelten Flächen. – Z. Pflanzenernaehr. Bodenk. **160**, 41–46, DOI:10.1002/jpln.19971600109.

Wessolek, G., B. Kluge, T. Nehls, B. Kocher, 2009: Aspekte zum Wasserhaushalt und Stofftransport urbaner Flächen [Aspects of water balance and solute transport of urban surfaces]. – Korrespondenz Wasserwirtschaft **2**, 205–210.

Wienert, U., W. Kuttler, 2005: The dependence of the urban heat island intensity on latitude A statistical approach. – Meteorol. Z. **14**, 677–686, DOI:10.1127/0941-2948/2005/0069.

Williams, A.P., R.E. Schwartz, S. Iacobellis, R. Seager, B.I. Cook, C.J. Still, G. Husak, J. Michaelsen, 2015: Urbanization causes increased cloud base height and decreased fog in coastal Southern California. – Geophys. Res. Lett. **42**, 1527–1536, DOI:10.1002/2015GL063266.

Wouters, H., K. de Ridder, L. Poelmans, P. Willems, J. Brouwers, P. Hosseinzadehtalaei, H. Tabari, S. van den Broucke, N.P.M. van Lipzig, M. Demuzere, 2017: Heat stress increase under climate change twice as large in cities as in rural areas: A study for a densely populated midlatitude maritime region. – Geophys. Res. Lett. **44**, 8997–9007, DOI:10.1002/2017GL074889.

Wright, C.Y., D.J. du Preez, B.S. Martincigh, et al., 2020: A comparision of solar ultraviolet radiation exposure in urban canyons in Venice, Italy and Johannesburg, South Africa. – Photochem. Photobiol. **97**, 1391–1396, DOI: 10.1111/php.1391.

Yahia, M.W., E. Johansson, S. Thorsson, F. Lindberg, M.I. Rasmussen, 2018: Effect of urban design on microclimate and thermal comfort outdoors in warm-humid Dar es Salaam, Tanzania. – Int. J. Biometeorol. **62**, 373–385, DOI: 10.1007/s00484-017-1380-7.

Yoshino, M., 1990/1991: Development of urban climatology and problems today. – Energy Build. **15-16**, 1–10.

Zhao, L., M. Oppenheimer, Q. Zhu, J.W. Baldwin, K.L. Ebi, E. Bou-Zeid, K. Guan, X. Liu, 2018: Interactions between urban heat islands and heat waves. – Env. Res. Lett. **13**, 34003, DOI:10.1088/1748-9326/aa9f73.

Zhou, B., D. Rybski, J.P. Kropp, 2013: On the statistics of urban heat island intensity. – Geophys. Res. Lett. **40**, 5486–5491, DOI:10.1002/2013GL057320.

Ziska, L.J., F. Caulfield, 2000: The potential Influence of rising atmospheric carbon dioxide (CO_2) on public Health: Pollen Production of Common Ragweed as a Test Case. – World Resour. Rev. **12**, 449–457.

Ziska, L.J., D.E. Gebhard, D.A. Frenz, et al., 2003: Cities as Harbingers of Climate Change: Common Ragweed, Urbanization, and Public Health. – J. Allergy Clinical Imm. **111**, 2, 290–295.

Zmarsly, E., W. Kuttler, H. Pethe, 2007: Meteorologisch-klimatologisches Grundwissen. Eine Einführung mit Übungen, Aufgaben und Lösungen; 34 Tabellen. – Ulmer, Stuttgart, 182 pp.